24059-6003-RU-00

(NASA-CR-142185) PHYSICS OF SUB-MICRON
COSMIC DUST PARTICLES Final Report (TRW
Systems Group) 56 p HC $4.25   CSCL 03B

N75-19101

                                                      Unclas
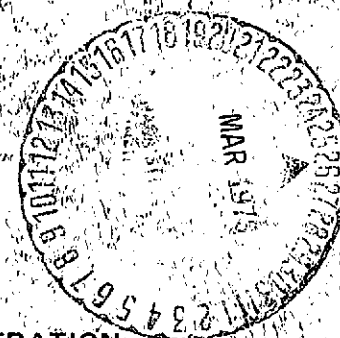   G3/90   17366

PHYSICS OF SUB-MICRON
COSMIC DUST PARTICLES

FINAL REPORT

by

N. L. Roy

TRW
SYSTEMS GROUP

ONE SPACE PARK • REDONDO BEACH, CALIFORNIA 90278

PHYSICS OF SUB-MICRON COSMIC DUST PARTICLES

FINAL REPORT

by

N. L. Roy

TRW
SYSTEMS GROUP

ONE SPACE PARK • REDONDO BEACH, CALIFORNIA 90278

PHYSICS OF SUB-MICRON COSMIC DUST PARTICLES

FINAL REPORT

October 1974

Prepared by: _N. L. Roy_
N. L. Roy
Chemical Physics Group
Systems Group Research Staff

Approved by: _C. Knox_
C. Knox
Director
Systems Group Research Staff

ABSTRACT

Laboratory tests with simulated micrometeoroids to measure the heat transfer coefficient are discussed. Equations for ablation path length for electrically accelerated micrometeoroids entering a gas target are developed which yield guidelines for the laboratory measurement of the heat transfer coefficient. Test results are presented for lanthanum hexaboride (LaB_6) microparticles in air, argon, and oxygen targets. The tests indicate the heat transfer coefficient has a value of approximately 0.9 at 30 km/sec, and that it increases to approximately unity at 50 km/ sec and above. Test results extend to over 100 km/sec. Results are also given for two types of small particle detectors. A solid state capacitor type detector was tested from 0.61 km/sec to 50 km/sec. An impact ionization type detector was tested from 1.0 to 150 km/sec using LaB_6 microparticles.

TABLE OF CONTENTS

LIST OF ILLUSTRATIONS

LIST OF ILLUSTRATIONS (continued)

1.0   INTRODUCTION

It would be desirable to characterize the entry conditions of microparticles into the earth's atmosphere with sufficient assurance to identify the various observable phenomena which are associated with such events. If the particle parameters along a micrometeoroid trail through the upper atmosphere could be completely specified, then a number of the meteor observable phenomena could be estimated. Two of the phenomena associated with micrometeoroid entry are atom deposition and ion deposition. Definition of these properties for an aribtrary meteoroid, and hence, for the total meteoroid flux into the earth's atmosphere, would lead to estimates of number densities as a function of altitude for the expected meteoroid elemental constituents. Correlation studies with high altitude measurements of the same elements could be used to either support or refute such estimates.

Another area of considerable interest to some observers is that of residual particulates. These too could be predicted with detailed knowledge of the meteoroid energy balance and ablation characteristics along its entry path. Estimates of size and number density as a function of altitude would permit correlation studies with high altitude collection experiments already performed, or would suggest altitudes at which future collection experiments should be made.

To be able to define the observable phenomena above, one needs to be able to specify energy balance in an arbitrary microparticle during entry. A number of associated parameters are important in this quest, but two are of particular significance: One quite important parameter is that of atmospheric density as a function of altitude. This is currently reasonably well defined from the many rocket and satellite measurements made in recent years. A second parameter, which requires better definition, is that of the heat transfer coefficient. Defining this coefficient, with assurance of its accuracy, is essential to meaningful calculations to attempt to quantify the observable phenomena of atom deposition, ion deposition, and especially residual particulates.

One of the major objectives of the present program was to determine the value of the heat transfer coefficient as it relates to micro-

particles entering a gaseous medium. The particular interest is in measuring the heat transfer coefficient which is most likely to prevail for micrometeoroids entering the upper atmosphere under conditions of unshielded impact. This is a condition where the mean free path of the gaseous elements exceeds the body dimensions of the micrometeoroid. If interest is confined to micron size and below this condition is satisfied at pressures below about 50 Torr for standard atmospheric constituents.

Initially, the objective was to perform a laboratory measurement of the heat transfer coefficient for ablating micrometeoroids in unshielded impact following the general experimental procedure used by Friichtenicht[1] and extend this work to higher velocities. This particular work predicted the effective value of the heat transfer coefficient to be approximately 0.7 at 24 km/sec and decreasing more or less linearly with velocity to a value of about 0.4 at 36 km/sec. Since the initial velocity of micrometeoroids could extend considerably higher than that investigated, measurement of the value of the coefficient at higher velocities could be of importance to the field of meteor physics, in general, and it would relate specifically to the problem of specifying micrometeoroid observable phenomena.

The method used by Friichtenicht was an optical one whereby a phototube viewed the ablation path of the particle. It had been established by previous experiment that the light emitted by an ablating particle was proportional to the mass lost by the particle. Therefore, by observing the ablation path of the particle, the mass of the ablating particle may be determined at any arbitrary point along the path. Once this is obtained then the cross-sectional area of the particle is known and hence, the energy input by collision with the gas molecules.

This technique works fine as long as the light emitted remains proportional to the mass lost by the particle. However, when high velocity microparticles are being observed with fixed ablation path lengths on the order of one meter, this condition may no longer hold. The reason the assumption no longer holds is that the mean free path of

the ablated atoms may exceed the experimental chamber dimensions at the lower gas pressures required. When this occurs thermalization of the emitted atoms cannot occur before the chamber walls are encountered, and consequently, the light emitted will no longer be proportional to the mass lost. The question is at what point does the assumption fail?

In Section 2.0 this question is addressed and equations are derived to show the validity of the assumption. Ablation path lengths are found in terms of the parameters of the particle and gas target. Equations are also derived which relate ablation path length to electrically accelerated microparticles. Equations are also found relating ablation path length to mean free path of the ablated atoms. These equations show directly the validity of the foregoing assumption and experimental guidelines are developed.

Using the guidelines developed, experiments were performed to measure the heat transfer coefficient from about 30 km/sec to 100 km/sec. The results of these experiments are presented in Section 3.0 along with a description of the experimental configuration and procedure.

In Section 4.0 small particle detectors are discussed and the test results for two types are presented. One is a capacitor type detector and the other utilizes impact ionization. Graphs are presented to show the sensitivity of each as functions of the impacting particle radius and velocity.

2.0   ABLATION PATH LENGTH FOR SIMULATED MICROMETEOROIDS ENTERING
       A GAS TARGET

2.1   General Considerations

The objective of the following article is to determine the
trail or path length required to completely vaporize a micrometeoroid
under given entry conditions. The micrometeoroid (particle) vaporization
or ablation characteristics surrounding such conditions have become of
interest, especially since they relate directly to laboratory experiments
in which the heat transfer coefficient of an ablating particle is to be
measured by optically viewing the excitation of the target gas caused by
ablated particle atoms. In such an experiment, the light emitted at any
instant along the particle path is assumed to be proportional to mass
lost by the particle at that point. If the assumption is correct and
can be measured under known conditions, then the heat transfer coefficient
may be determined.[1] The particular question to be addressed is at what
point or under what conditions does the original assumption become
invalid. Clearly, if the visible excitation of the target gas along the
particle path is to be at all points proportional to the mass lost, then
all ablated atoms must be completely thermalized at or near the position
at which they were ejected. Complete thermalization may require a large
number of collisions since the kinetic energy of the ablated atoms may
be on the order of 1000 electron volts or more. By determining the re-
quired ablation path length for the particular parameters of interest,
some insight will be gained regarding the validity of the foregoing
assumption.

Equations will be developed in terms of the pertinent para-
meters to answer the above question and these should prove to be of
further use in the practical design of a laboratory experiment to measure
the heat transfer coefficient. Particular emphasis will be made on those
conditions relating to the use of particles obtained by electrostatic
acceleration in a microparticle accelerator. Since several expressions
will involve electrostatic acceleration, it will be most convenient to
use the MKS system of units except where specified otherwise.

2.2   Calculation of Ablation Path Length

In determining the path length (L) required to produce complete vaporization of an incident particle, the incremental mass loss relation is needed as a function of distance along the path. To achieve this, the increment of energy expended to vaporize an element of mass is equated to that available by collision with the gas molecules incident upon the surface of the particle. The relation is

$$\xi dm = \frac{1}{2} \gamma A \rho_g v^3 \, dt \tag{1}$$

where,

ξ = total energy required to heat and vaporize a unit of mass,

dm = mass element vaporized,

γ = heat transfer coefficient = fraction of available energy expended on heating and vaporization,

ρ_g = density of gas along the path,

v = velocity of the particle relative to the gas,

dt = time element during which mass dm is vaporized.

Equation (1) above assumes that the energy expended by radiation is negligibly small. The relative magnitude may be illustrated by considering an iron particle of radius 1.0 micron, initial velocity of 20 km/sec or higher, and ablation path length of 1.0 meter, as an example. The radiated energy for this case can be shown to be less than 1.0 percent of the total energy required for vaporization of the particle.

If consideration is limited to spherical particles, a relation can be found in terms of the radius (r) and density of the particle material (ρ_p) since,

$$m = \frac{4}{3} \pi \rho_p r^3 \quad . \tag{2}$$

Then, $$dm = 4\pi \rho_p r^2 dr \quad . \tag{3}$$

If the deceleration of the particle is small during the time ablation occurs then the velocity (v) may be considered constant over this inter-val. (This is a relatively good approximation for high velocity particles since the kinetic energy exceeds by many times that required for ablation). Then the relation between the time (t) and distance (x) traveled is simply

$$t = \frac{x}{v}$$

and

$$dt = \frac{dx}{v} \tag{4}$$

By substituting Equations (3) and (4) into Equation (1), an incremental relationship between dr and dx is obtained,

$$dr = - \frac{\gamma \rho_g v^2 dx}{8\xi \rho_p} \quad . \tag{5}$$

By integrating the above equation from the initial particle radius (r_0), which corresponds to $x = 0$, to the final radius (r_f), which corresponds to the point $x = L$, the following is obtained:

$$\int_{r_0}^{r_f} dr = - \frac{\gamma \rho_g v^2}{8\xi \rho_p} \int_0^L dx \tag{6}$$

$$r_0 - r_f = \frac{\gamma \rho_g v^2 L}{8\xi \rho_p} \tag{7}$$

By letting r_f go to zero, the desired expression for the ablation path length is obtained, which is

$$L = \frac{8\xi \rho_p r_0}{\gamma \rho_g v^2} \tag{8}$$

Equation (8) is valid for all cases where ablation is actually occurring and the change in particle velocity is small over the path length. For better visualization of the relation between gas density, path length, and particle velocity, the pressure of the gas target may

be substituted for gas density if the target gas is specified. Using air as a sample gas and the known gas density at a pressure of 1.0 micron of mercury (2.26×10^{-6} kg/micron-m^3, which is based on a collision cross-section of 3.1×10^{-19} m^2 and 28.8 amu average atomic mass), the target pressure P_0 is obtained from

$$P_0 = \frac{\rho_g}{2.26 \times 10^{-6}} \qquad (P_0 \text{ in microns}) \quad . \tag{9}$$

Substituting Equation (9) into Equation (8), an expression for P_0L is obtained,

$$P_0L = \frac{(3.54 \times 10^6)\xi\rho_p r_0}{\gamma v^2} \qquad (\text{micron-meters}) . \tag{10}$$

In Figure 2-1 the quantity P_0L is plotted against the square of the particle velocity for several values of the initial radius (r_0) as a running parameter when the ablating particle is iron with an assumed density (ρ_p) of 7.8×10^3 kg/m^3, total heat of vaporization (ξ) of 8.3×10^6 J/kg, and heat transfer coefficient (γ) of 1.0. It may be seen from the Figure, for example, that for $r_0 = 2 \times 10^{-8}$ meters and $v^2 = 4 \times 10^9$ m^2/sec^2 a P_0L value of approximately 1.0 is required. Therefore, an experimental arrangement having a 1.0 meter long target range will require only 1.0 micron of air pressure within to cause complete vaporization of the incident particle.

Figure 2-2 is a similar plot of P_0L versus particle velocity squared for lanthanum hexaboride particles. The density of the particles is assumed to be 2.61×10^3 kg/m^3. The heat of vaporization^2 is taken to be 3.48×10^6 J/kg and heat transfer coefficient (γ) = 1.0. For this material, a 2.0×10^{-8} meter radius particle with $v^2 = 4 \times 10^9$ m^2/sec^2 will undergo complete vaporization with a P_0L value of only 0.15 micron-meters.

2.3   Equations Relating to Electrostatically Accelerated Micro-particles

For ablation experiments involving the use of microparticles from an electrostatic accelerator, it may prove useful to have Equation
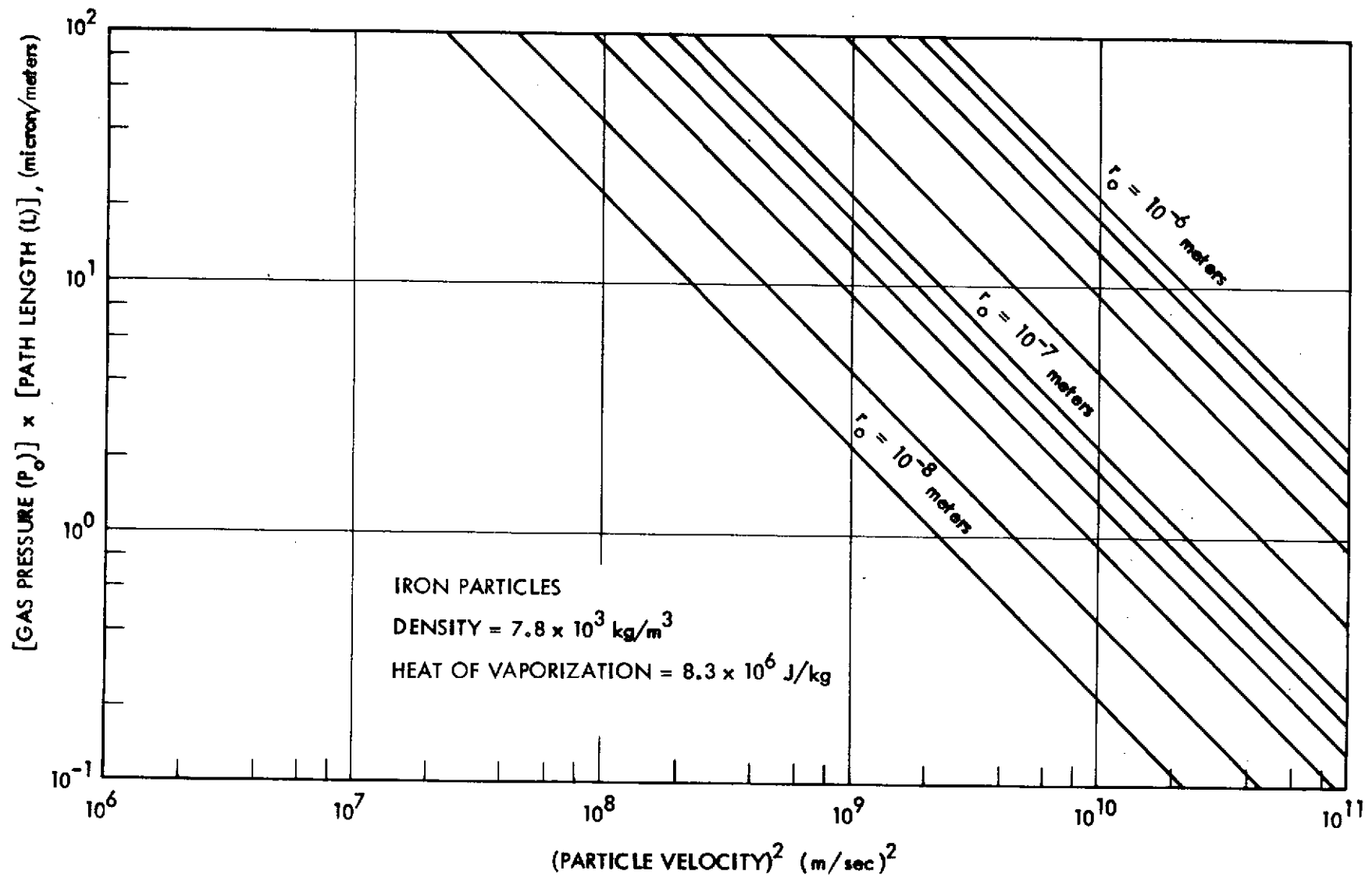
Figure 2-1. Gas Pressure (P_0) Times Path Length (L) vs Particle Velocity Squared for Iron Particles.

Figure 2-2. Gas Pressure (P_o) Times Path Length (L) <u>vs</u> Particle Velocity Squared for Lanthanum Hexaboride.

[GAS PRESSURE (P_o)] × [PATH LENGTH (L)], (micron/meters)

(PARTICLE VELOCITY)^2 (m/sec)^2

$r_o = 10^{-6}$ meters

$r_o = 10^{-7}$ meters

$r_o = 10^{-8}$ meters

LANTHANUM HEXABORIDE PARTICLES

DENSITY = 2.61×10^3 kg/m^3

HEAT OF VAPORIZATION = 3.48×10^6 J/kg

(8) rewritten in terms of the parameters of the accelerator. The mass (m) and velocity (v) may be expressed in terms of the particle charge (q) and total accelerating voltage (V_a) by equating the final kinetic energy of the particle to the potential energy available before undergoing acceleration which is

$$\frac{1}{2} mv^2 = qV_a \quad .$$

(11)

If consideration is limited to spherical particles, the charge (q) acquired by the particle is related to the obtainable surface electric field (E) and permittivity of free space (ε_0) by the relation

$$q = 4\pi E \varepsilon_0 r_0^2 \quad .$$

(12)

For spherical particles, Equation (2) again applies

$$m = \frac{4}{3} \pi \rho_p r_0^3 \quad .$$

(13)

Equation (13) may then be substituted into Equation (8) to obtain the path length (L) as a function of particle, gas, and accelerator parameters

$$L = \frac{4\xi \rho_p^2 r_0^2}{3\gamma \rho_g \varepsilon_0 E V_a} \quad .$$

(14)

Alternatively, Equation (13) may be substituted into Equation (10) to obtain

$$P_0 L = \frac{(5.90 \times 10^5)\xi \rho_p^2 r_0^2}{\gamma \varepsilon_0 E V_a} \quad \text{(micron-meters)} \quad .$$

(15)

Equation (13) was used to generate the graphs of available particle radii shown in Figures 2-3 and 2-4. The parameters assumed for the calculations are

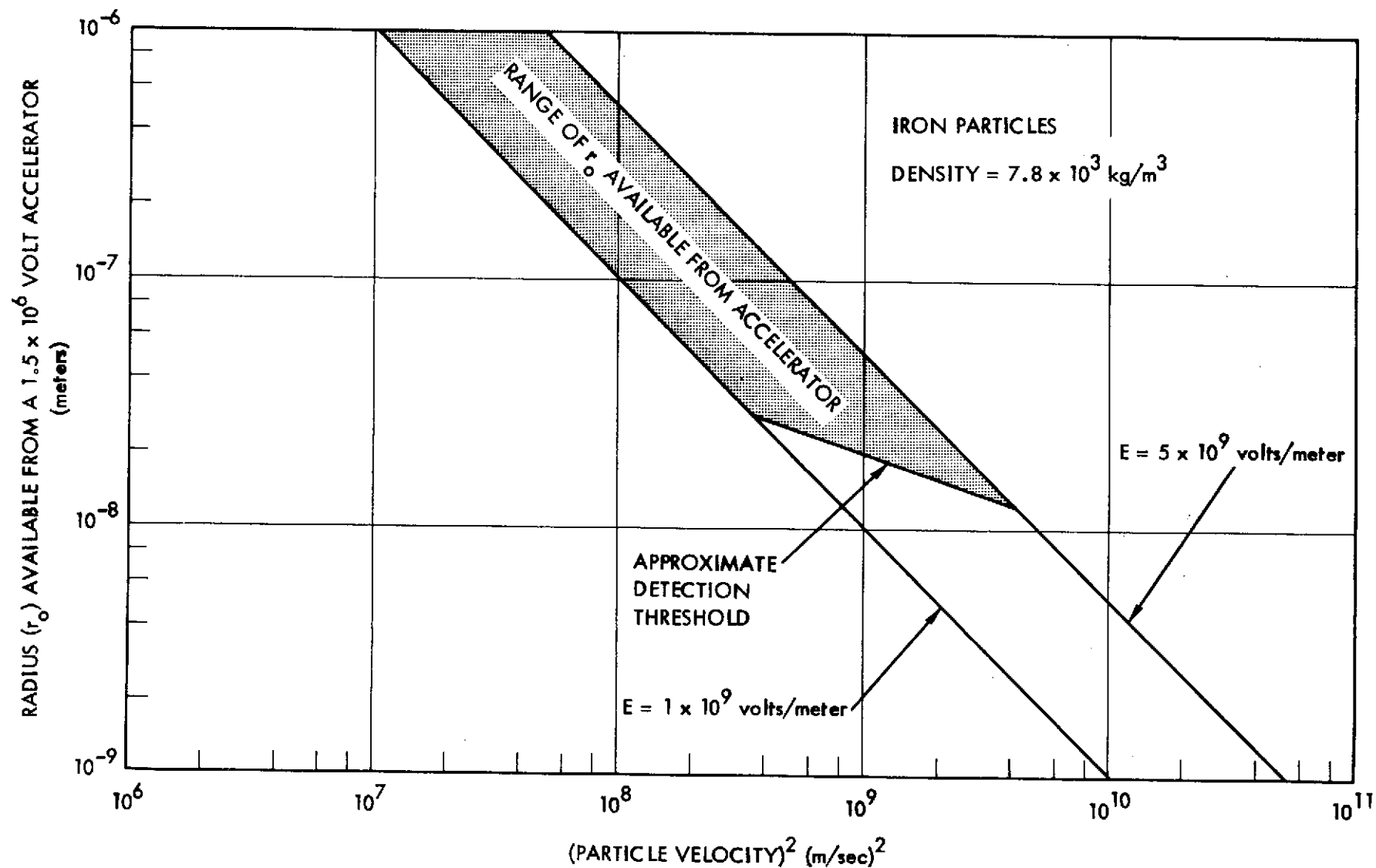$$\varepsilon_0 = 8.85 \times 10^{-12} \text{ farad/meter} \quad ,$$

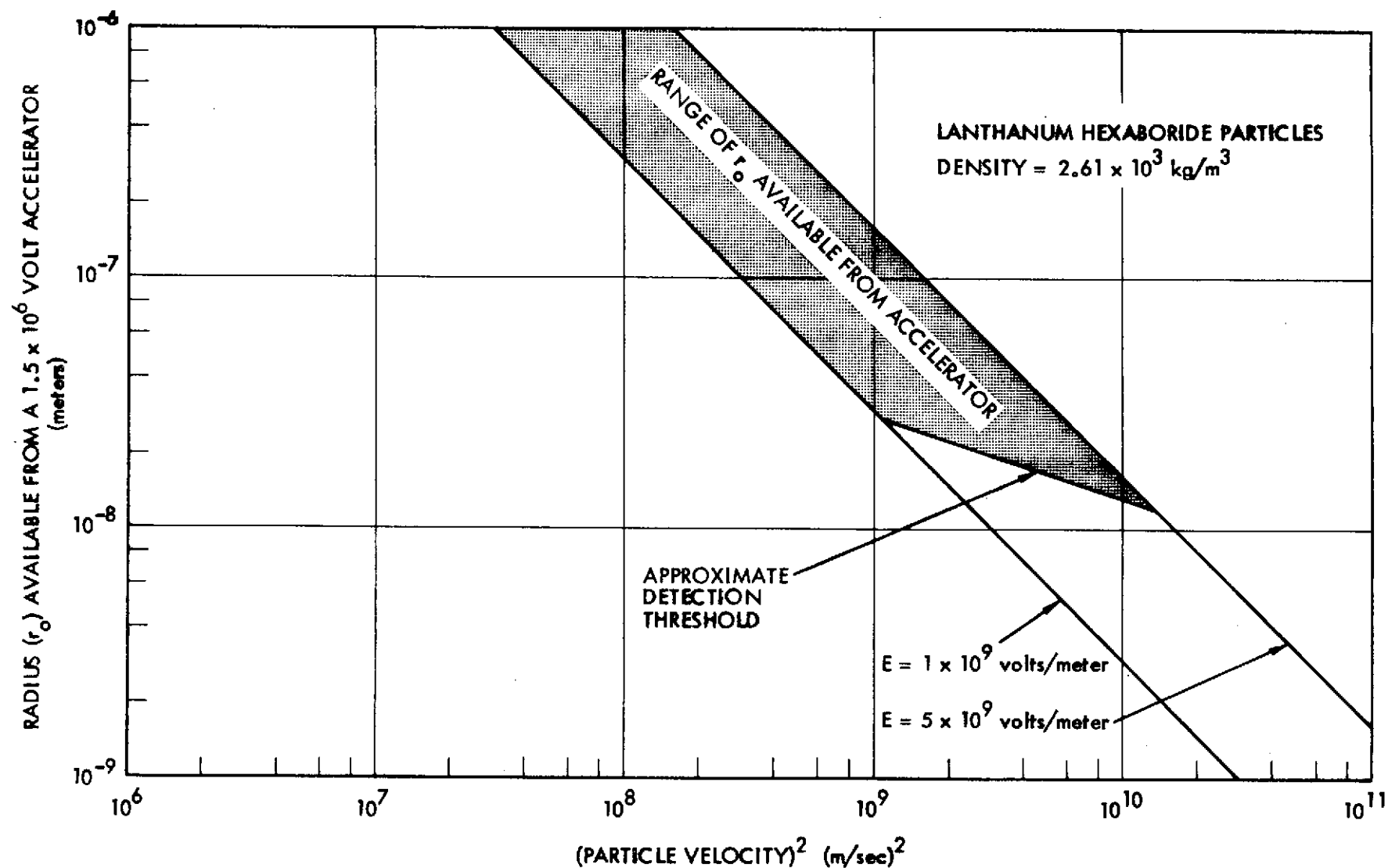Figure 2-3. Radius (r_0) Available From a 1.5×10^6 Volt Acclerator vs Particle Velocity Squared for Iron Particles.

Figure 2-4. Radius (r_o) Available From a 1.5 x 10^6 Volt Accelerator vs Particle Velocity Squared for Lanthanum Hexaboride Particles.

$$E = 1.0 \times 10^9 \text{ to } 5.0 \times 10^9 \text{ volts/meter},$$

$$V_a = 1.50 \times 10^6 \text{ volts},$$

$$\rho_p = 7.8 \times 10^3 \text{ kg/m}^3 \text{ (iron)},$$

$$\rho_p = 2.61 \times 10^3 \text{ kg/m}^3 \text{ (lanthanum hexaboride)}.$$

For any given particle velocity, the range of expected radii for either material may be determined from the cross hatched section and the left scale. In each case, the approximate detection threshold is indicated for the surface electric field strength (E) shown. For a given particle radius and surface field strength, the velocity obtained with lanthanum hexaboride is higher than that obtained with iron by the square root of the density ratio

$$\left(v_{LaB_6} = \left(\rho_{iron} / \rho_{LaB_6} \right)^{1/2} v_{iron} \right).$$

2.4 Mean Free Path Considerations

In certain laboratory experiments it becomes important to consider the mean free path for ablated atoms in the target gas. In experiments where complete thermalization of the ablated atoms is required, the experimental chamber dimensions must be sufficiently large to allow for several mean free path lengths for ablated atoms before the chamber walls are encountered. In the discussion to follow a relationship will be developed to relate the gas target mean free path to ablation path length and particle and accelerator parameters.

If the molecular diameters of the gas and ablated atoms are considered approximately the same, the mean free path (λ) of an ablated atom may be related to the molecular number density (n) and collision cross section (σ) by

$$n\sigma\lambda = 1.$$

<div style="text-align: right;">(16)</div>

The gas density ρ_g and molecular mass (μ) is related to n by

$$n = \frac{\rho_g}{\mu} \quad .$$

(17)

Substituting Equation (17) into Equation (16) gives

$$\lambda = \frac{\mu}{\sigma \rho_g} \quad .$$

(18)

An interesting ratio is obtained by dividing the path length (Equation (14)) by the mean free path (Equation (18)),

$$\frac{L}{\lambda} = \frac{4\sigma\xi\rho_p^2 r_o^2}{3\gamma\mu\epsilon_o EV_a} \quad .$$

(19)

The ratio L/λ is seen to be independent of gas density depending only upon the molecular mass. Figure 2-5 is a plot of L/λ versus r_o^2 for both iron and LaB_6 particles. The resultant shown is obtained using the following constants:

$$\sigma = 3.1 \times 10^{-19} \text{ m}^2 \quad ,$$

$$\xi = 8.3 \times 10^6 \text{ J/kg (iron)} \quad ,$$

$$\xi = 3.48 \times 10^6 \text{ J/kg } (LaB_6) \quad ,$$

$$\rho_p = 7.8 \times 10^3 \text{ kg/m}^3 \text{ (iron)} \quad ,$$

$$\rho_p = 2.61 \times 10^3 \text{ kg/m}^3 (LaB_6)$$

$$\gamma = 1.0 \quad ,$$

$$\mu = 4.81 \times 10^{-26} \text{ kg (28.8 amu)} \quad ,$$

$$\epsilon_o = 8.85 \times 10^{-12} \text{ farads/meter} \quad ,$$
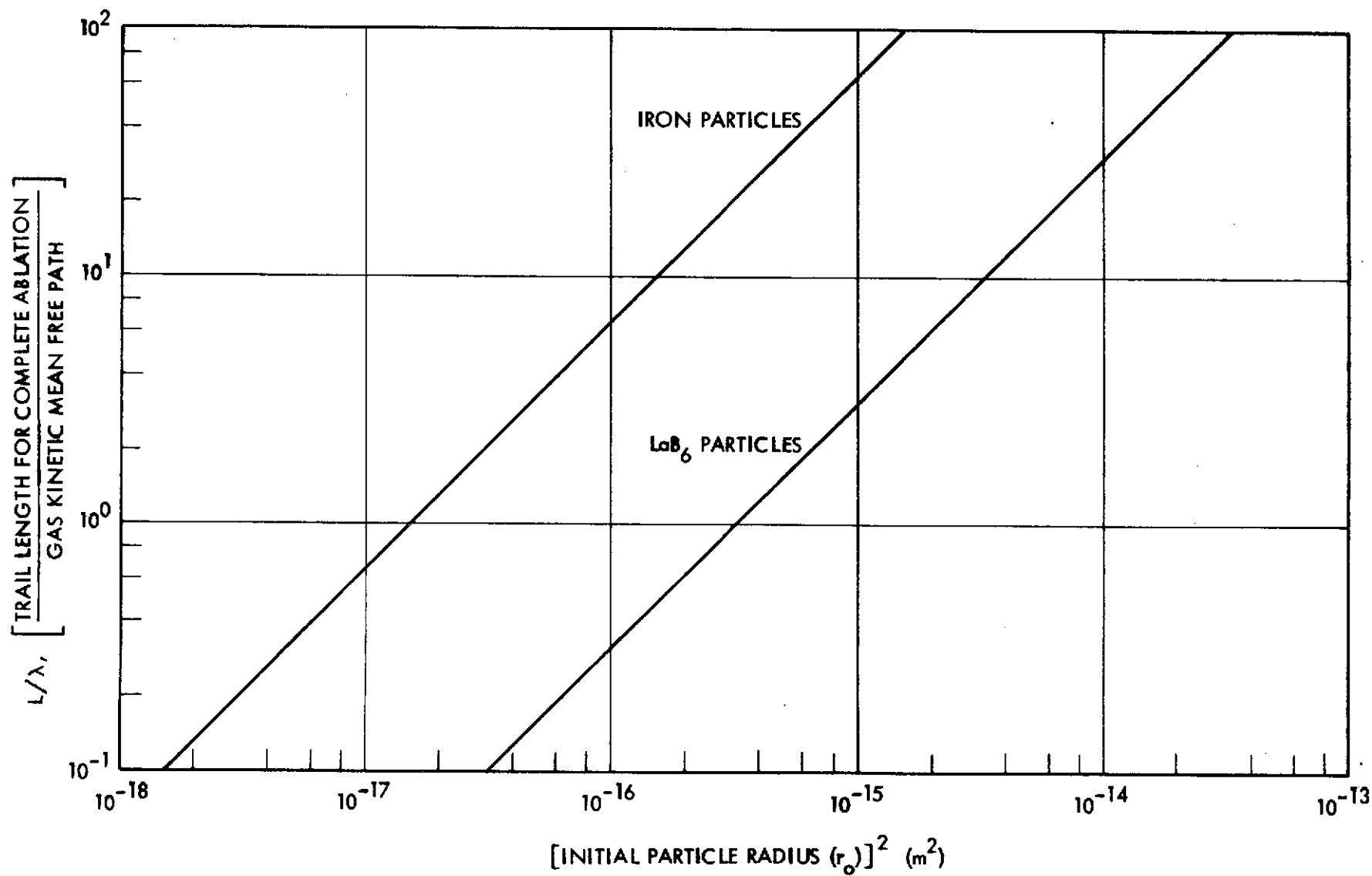
Figure 2-5. L/λ vs Initial Particle Radius (r_o) Squared for Iron and Lanthanum Hexaboride Particles.

$$E = 5 \times 10^9 \text{ volts/meter} ,$$

$$V_a = 1.5 \times 10^6 \text{ volts} .$$

From Figure 2-5 one can see that particles having the radii shown from an electrostatic accelerator with the above characteristics will vaporize completely in a very small number of mean free path lengths.

The L/λ ratio as a function of particle velocity is perhaps of more interest. This may be obtained by noting that Equation (13) gives v^2 as a function of r_0 which may be rearranged and squared to yield

$$\rho_p^2 \, r_0^2 = \frac{36\varepsilon_0^2 E^2 V_a^2}{v^4} \tag{20}$$

Substitution of the value of $\rho_p^2 \, r_0^2$ of Equation (20) into Equation (19) yields the desired equation for L/λ as a function of particle velocity,

$$\frac{L}{\lambda} = \frac{48\sigma\xi\varepsilon_0 E V_a}{\gamma\mu v^4} . \tag{21}$$

Figure 2-6 illustrates Equation (21) in graphical form for the same parameters given previously for Figure 2-5. It may be seen that iron particles will vaporize completely in less than 10 mean free path lengths above 64 km/sec while the corresponding velocity for LaB_6 particles is about 52 km/sec. Furthermore, LaB_6 particles will vaporize completely in one mean free path length at 93 km/sec while the same occurs for iron at 114 km/sec.

2.5   Discussion of Experimental Guidelines Obtained

In the above sections, equations were developed which illustrate the most probable conditions required for complete ablation of sub-micron size range particles entering an air target gas. Particular emphasis was given to particles of iron and lanthanum hexaboride microparticles obtained by electrostatic acceleration. The equations and graphical presentations should be beneficial in the implementation of possible laboratory experiments designed to function in the regimes studied.
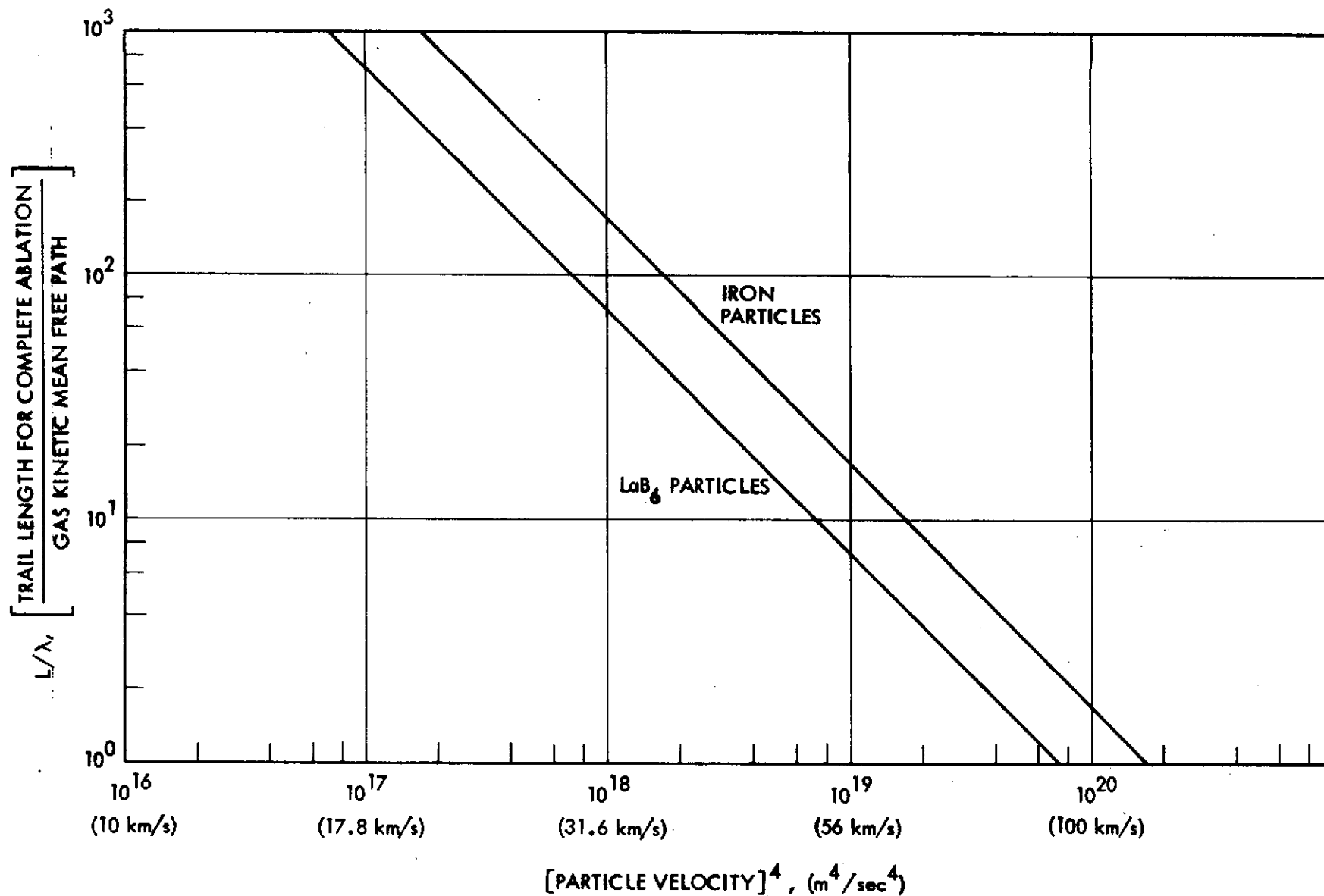
Figure 2-6. L/λ vs Particle Velocity to the Fourth Power for Iron and Lanthanum Hexaboride Particles.

The particular question asked at the beginning, regarding the conditions under which an optical experiment of the nature described becomes invalid, may now be answered, in general, from the information given in Figure 2-6. For nearly complete thermalization of the ablated atoms near the point at which they were ejected, an ablation path extending several hundred mean free path lengths is required. This criterion implies that significant error may occur in such measurements at velocities near or exeeding about 30 km/sec for the conditions used in preparation of Figure 2-6.

3.0   LABORATORY MEASUREMENT OF THE HEAT TRANSFER COEFFICIENT

3.1   Experimental Objective and Procedures

Initially, the experimental objective was to measure the heat transfer coefficient in the laboratory using high velocity microparticles in much the same manner as that used by Friichtenicht.[1] Due to advances in the acceleration and detection of microparticles, it was felt that the coefficient could be measured to velocities considerably higher than the 35 - 40 km/sec attained in the previous work. This objective seemed to be of particular importance since the indication was that the coefficient had a sharply decreasing value with velocity and therefore could have considerable impact to the field of meteor physics.

The analysis of ablation path length in a gas target, presented in Section 2.0, showed that the optical procedure used previously could not be extended to velocities above about 30 km/sec due to the long mean free path lengths which accompany the low gas densities required for ablation within the desired region. For the velocity range of interest (30 km/sec to 100 km/sec) an alternative method of measurement would be required.

The equation derived for ablation path length in Section 2.2 (Equation (8); $L = (8\xi\rho_p r_o)/(\gamma\rho_g v^2)$) indicated an alternative if the path length (L) could be determined. If (L) could be measured then all other quantities except the coefficient (γ) could be either measured directly in the laboratory or were known constants. Since optically viewing the particle track has already been shown to be invalid in the velocity range of interest, there seemed to be no obvious way to measure an arbitrary path length for ablation. However, if the particle radius (r_o), particle velocity (v), and the gas density (ρ_g) could be adjusted in such a way as to make (L) fixed in value, then a method is available to show when the particle mass approaches zero. The technique is to use the ionization produced by impact of a solid particle as a tag to indicate a non-zero residual mass. Considerable work has been done in the area of impact ionization all of which has shown the method to be an extremely sensitive one for detecting the presence of a high velocity solid mass.[3,4] As will be shown later in Section 4.3, impact of a solid

particle with a tungsten plate at 10 km/sec produces impact ionization of approximately 10^4 coulombs/kilogram. The quantity of impact ionization produced rises to about 10^7 coulombs/kilogram at 100 km/sec. Standard charge detectors used in the TRW Microparticle Accelerator Facility have an equivalent noise charge on the order of 10^{-16} coulombs. Hence, one could expect to detect a residual mass on the order of 10^{-20} kg at 10 km/sec and 10^{-23} kg at 100 km/sec.

The approach described above is the one which was used to obtain the results to be presented later in this section. High velocity microparticles are admitted to a gas target region where the gas density may be varied as required to produce complete vaporization of the incident particle. The presence of residual mass is indicated when an ionization signal is produced at a time coinciding with impact of the particle with the detector element. A more detailed description of the experiment follows in Section 3.2.

3.2   The Experimental Facility

3.2.1   The Micrometeoroid Accelerator and Associated Apparatus

Several different experiments will be described in this section and Section 4.0 which involve the use of high velocity microparticles. Since a knowledge of the experimental arrangement is essential for ease of interpretation of the various data to be presented, a general description of the apparatus will be given. The discussion to follow is brief but will hopefully be adequate for the purpose intended. Should more detailed information be desired, a number of technical papers have been published regarding technical aspects of several of the subsystems employed. These will be referenced at appropriate points.

Figure 3-1 is a block diagram of the general experimental arrangement used for the tests conducted on this program. The description here will be limited to the general accelerator and the supporting subsystems which are used to detect and select the desired microparticles from the accelerator. A detailed description of the gas target and associated equipment will be given in the next subsection.

The particle accelerator is a two million volt Van de Graaff generator in which the high voltage terminal has been modified to accept
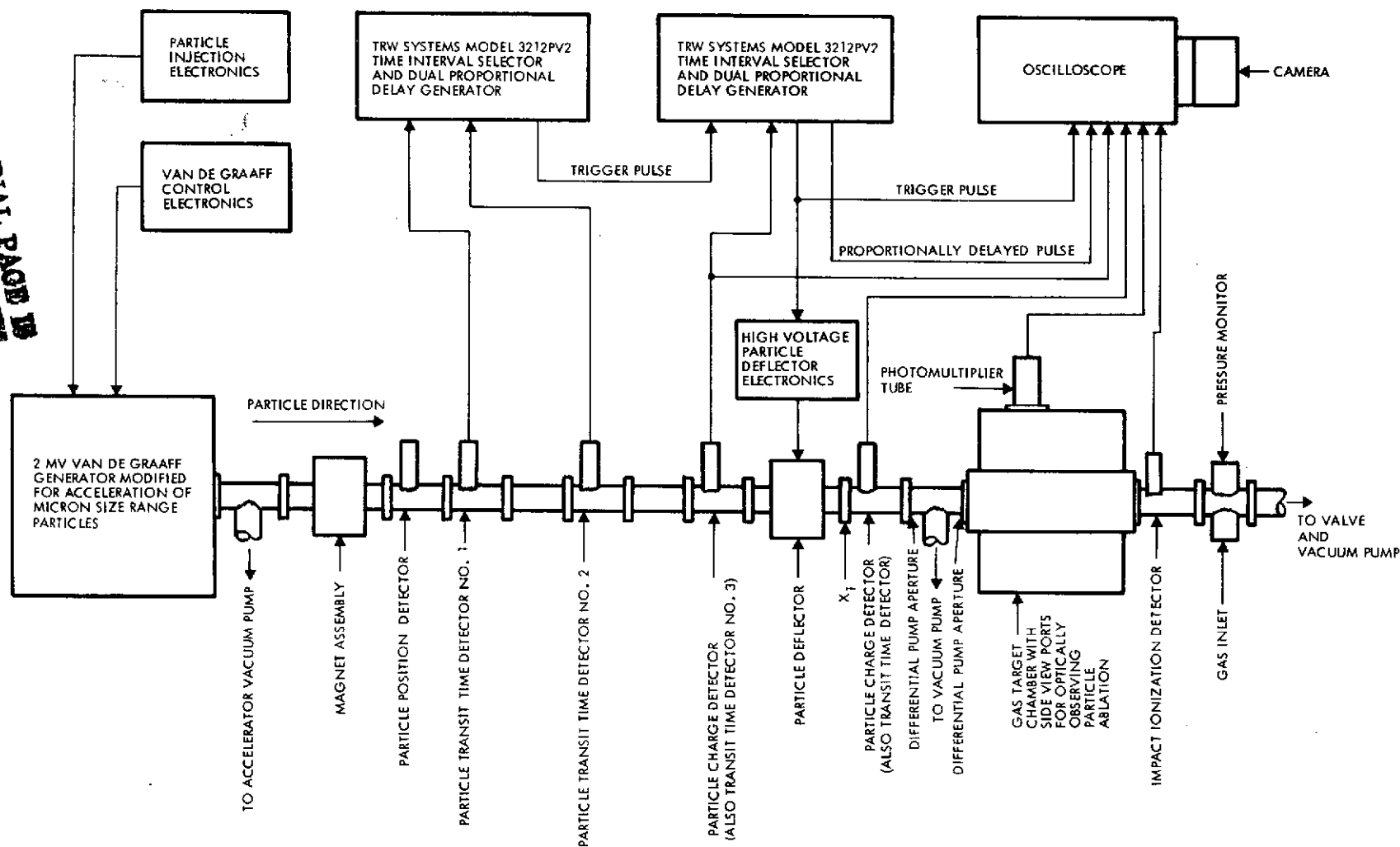
Figure 3-1. Block Diagram of TRW Systems Group Micrometeoroid Simulation and Test Facility, Showing Setup for Heat Transfer Measurement.

microparticle charging and injection equipment.[5] This equipment is
capable of charging and accelerating a variety of micron and sub-micron
size range materials to high velocities. The final velocity obtained is
dependent upon the size of the particular particle, the material used,
and the accelerating potential. Particle velocities range down to below
one kilometer per second for all materials. The upper velocity limit is,
for practical purposes, dependent upon the electronics used for particle
detection. For carbonyl iron particles and the particle detectors pre-
sently used in this facility, the maximum detectable velocity is about
80 km/sec; for lower density materials, the maximum detectable velocity
is much higher. (For example, data using lanthanum hexaboride (ρ_p = 2.61)
particles are presented later in this report and extends to 150 km/sec).
Particles may be accelerated either continually or in single bursts.

Particles exiting from the accelerator first pass through a
magnet assembly where ions, which may have been produced by the charging
process, are removed. A particle position detector[6] then provides a means
for locating the particle "beam" axis in order to align the system. The
particles next pass through two detectors spaced apart a carefully
measured distance from which the transit time over this distance may be
measured. The time separation of the two detector signals is analyzed
by a TRW Systems Model 3212PV2 Time Interval Selector and Dual Proportion-
al Delay Generator.[7] The principal function of this unit is to provide
an output pulse which is time coincident with the detection of the
particle in Transit Time Detector No. 2, when the measured transit time
falls within the bounds of some predetermined time interval. This pulse
is used as a trigger pulse and is fed to the No. 1 input of a second
Time Interval Selector and proportional Delay Generator whose internal
functions are identical with those of the first unit. A third transit
time detector spaced a carefully measured distance downstream from the
second transit time detector produces a pulse upon arrival of the charged
particle at that location. This pulse is fed to the No. 2 input of the
second Time Interval Selector. This unit has two principal functions:
First, it provides an output trigger pulse which is time coincident with
the detection of the particle in Transit Time Detector No. 3 when the
measured transit time between detectors No. 2 and No. 3 falls within some

predetermined time interval. This pulse is used to trigger an oscillo-
scope sweep and is also used to trigger a particle deflector. Normally,
with no signal applied to the input of the particle deflector high voltage
electronics, all particles are deflected by a bias voltage on a pair of
deflector plates and are not allowed to continue downstream toward the
experimental area. A signal from the Time Interval Selector removes the
bias voltage for a time just sufficient to allow the selected particle
to pass. The selected particle continues downstream through a sensitive
particle charge detector[8] and into the experimental area. Second, the
Time Interval Selector contains proportional delay generators which produce
two trigger pulses at adjustable multiples of the actual measured transit
time between detectors No. 2 and No. 3. By proper adjustment of the
multipication factors, these pulses can be made to appear when the
selected particle is at two arbitrarily selected points downstream, inde-
pendent of particle velocity. Only one of the two available proportionally
delayed pulses is used in the diagram shown. It is used to start the No.
2 beam of a dual beam oscilloscope and is normally set to occur when the
particle is at position x_1, which is just prior to the particle entering
the charge detector which precedes the differential pump section.

From the description above it should be clear that if the two
Time Interval Selectors are set to select identical transit times and the
distance between detectors No. 1 and No. 2 is the same as that between
No. 2 and No. 3, then a double coincident circuit is produced to control
particle transmission through the particle deflector. This particle
selection configuration has very high noise rejection and permits both
of the Time Interval Selectors to work very close to the detector noise
level without producing spurious trigger pulses to the selection and re-
cording equipment.

3.2.2 Experiment Configuration

The last particle charge detector, differential pump section,
and gas target region with associated equipment are depicted schematically
in Figure 3-2. The direction of particle flow is from left to right in
this figure. Particles entering the experimental region from the left
of the figure have been velocity selected by the equipment described in

TO OSCILLOSCOPE

PHOTOMULTIPLIER TUBE
POSITIONED TO VIEW
ENTIRE GAS TARGET
REGION

PMT

TO + 150 VOLT
BIAS SUPPLY

TO
OSCILLOSCOPE

TO
OSCILLOSCOPE

LIGHT TIGHT
ENCLOSURE

AMPLIFIER

AMPLIFIER

MKS
BARATRON
PRESSURE
GAUGE

LAST
PARTICLE
CHARGE
DETECTOR

WINDOW

GAS TARGET REGION

PARTICLE DIRECTION

TO VALVE
AND
DIFFUSION
PUMP

TO OTHER
PARTICLE
DETECTORS
AND
VAN DE GRAAFF

WINDOW

0.100 APERTURES
FOR DIFFERENTIAL
PUMP SECTION

TO VACUUM PUMP
(DIFFUSION PUMP)

IMPACT IONIZATION TARGET
AND GRID ASSEMBLY

TO-150 VOLT
BIAS SUPPLY

TO GAS
SUPPLY

LIGHT TIGHT ENCLOSURE
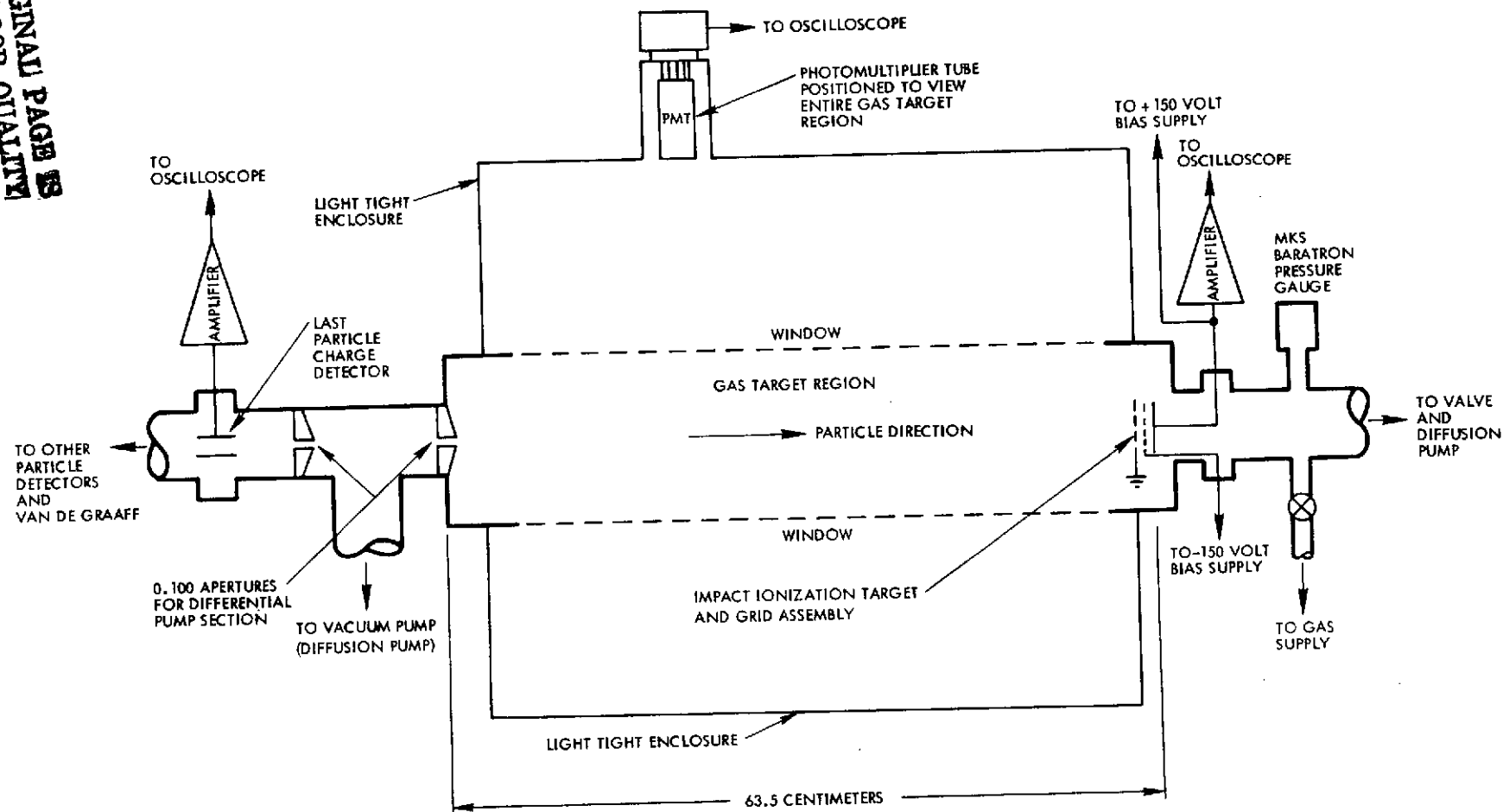
63.5 CENTIMETERS

Figure 3-2.   Schematic Diagram of the Gas Target Assembly and Associated Equipment.

Figure 3-1. Normally, a trigger pulse would be provided by the second Time Interval Selector just as the particle enters the diagram which would be used to trigger a second beam on a dual beam oscilloscope. This triggering method permits the transit of the particle through the charge detector and the gas target chamber to be displayed on a relatively fast sweep speed if desired.

After passing through the last particle charge detector, the selected particle traverses a differentially pumped section where the particle must pass through two 0.100 inch diameter apertures. The two apertures together with the included pump section effectively isolates the high vacuum portion of the accelerator from the relatively high pressure of the gas target region. After passing through the second aperture, the selected particle is subjected to a region of constant pressure where heating and ablation occur. The light emitted by the passage of the particle is observed through a window by the photomultiplier tube shown at the top center of the figure. The resulting signal is not used in a quantitative sense for this experiment but does provide a positive indication that the particle successfully traversed the aperture in the pump section.

If the pressure in the target region is too low to cause complete evaporation of the incident particle, then a portion of the still solid core of the particle will strike the impact ionization target plate at the right end of the chamber. As indicated, the path length through the gas target to this point is 63.5 centimeters. Such a particle will produce an observable impact signal which indicates incomplete evaporation. Should the incident particle completely evaporate just prior to impact then only single atoms will strike the plate and will produce no observable output signal. (In some cases, especially at high velocities, a cloud of ions will arrive at the target plate with sufficient energy to pass through the biased grid assembly and will produce a signal. As will be seen later in some of the oscilloscope photographs of the particle transit, the ion signal is spread out in time and is easily separated from the abrupt stop function caused by solid particle impact).

The pressure in the target region is maintained by a precision leak valve which permits adjusting the input flow rate from the gas supply to balance that lost through the differential pump aperture. The dimensions of the target region are large and no significant pressure drop occurs across the length of the chamber due to this small flow. The valve and diffusion pump to the right of the figure permit the chamber pressure to be reduced to below 10^{-5} Torr and provides the hard vacuum conditions needed for the impact ionization measurements which will be shown in Section 4.3. The pressure in the chamber was monitored by an MKS Baratron which was referenced to a hard vacuum of approximately 10^{-6} Torr.

The impact ionization detector consisted of a tungsten target plate and the two grids shown in Figure 3-2. The outermost grid was at ground potential to prevent electrical fields from the biased internal elements from extending beyond its mounting location. The internal grid was biased at -150 volts to prevent electrons formed in the ablation process from reaching the target plate. The target plate was biased to +150 volts. This bias voltage prevents ions of less than 150 volts from reaching the detector plate and also combines with the -150 volts on the inner grid to form a 300 volt drop across the 0.6 centimeter spacing.

3.3   Experimental Results

3.3.1   Discussion of Recorded Data

Lanthanum hexaboride particles were selected for use in the heat transfer measurements solely because of low density and ease of operation in the electrostatic accelerator. The density of LaB_6 (2.61 gms/cm^3) permits detection of particles up to 150 km/sec which covers quite adequately the current region of interest. Iron, on the other hand, may have been of more interest as a material but the data would have extended to only 80 km/sec due to the higher density. The LaB_6 particles were obtained from Cerac, Inc., Butler, Wisconsin. The fabrication process is proprietary but is believed to be a form of grinding since the particles are irregular in shape. Spherical particles were desired but were unavailable.

Figure 3-3 contains four oscilloscope photographs which are representative of typical data acquired at approximately 20 km/sec and 50 km/sec. Figure 3-3a illustrates a 5.18 km/sec particle having a mass of 2.08×10^{-18} kg traversing the chamber with 1.0×10^{-3} Torr argon pressure. The upper trace consists of two rectangular pulses which are the signals from the first and second particle charge detectors. The time separation of these two pulses is used to measure particle velocity while the amplitude of the second pulse is used to measure particle charge. The transit time and particle charge together with the accelerator voltage are sufficient to calculate particle mass from the conservation of energy equation ($1/2 \ mv^2 = qV_a$; Equation (11)). After the second particle charge detector signal the upper trace is seen to increase positively which represents the integrated light collected by the photomultiplier tube (PMT) observing the particle track. Recall that this signal is used as a positive indication that the particle has entered the gas target region. Finally, a negative going pulse indicates arrival of charge at the impact ionization detector. The initial part of the signal is seen to increase slowly, in a negative direction, caused by the arrival of ions formed in the gas by impact and which have velocities higher than that of the particle. Shortly after the signal begins increasing negatively, an abrupt step occurs of very short risetime. This portion of the signal is produced by impact of a small amount of residual mass which was not evaporated. The remainder of the signal is ion current from ions which straggle along behind the particle.

The lower trace in the photograph starts just prior to the particle reaching the second particle charge detector. It then displays the second particle charge detector signal, the photomultiplier signal, and the impact ionization signal. The last two are at higher sensitivity than that used on the upper trace.

Figure 3-3b shows the signals from a particle with v = 51.3 km/sec, m = 1.30×10^{-18} kg, and argon gas pressure (P_o) = 1.5×10^{-3} Torr. This particular particle has undergone complete evaporation as evidenced by the complete absence of the sharp step in the signal which would be produced by particle impact on the target plate. The relatively wide
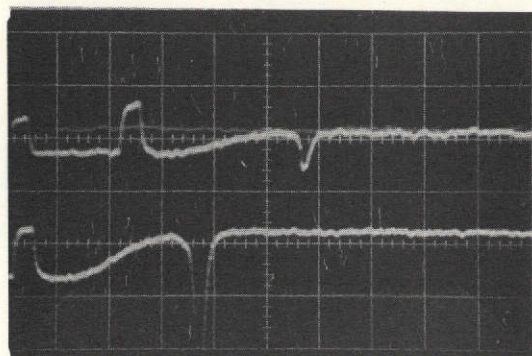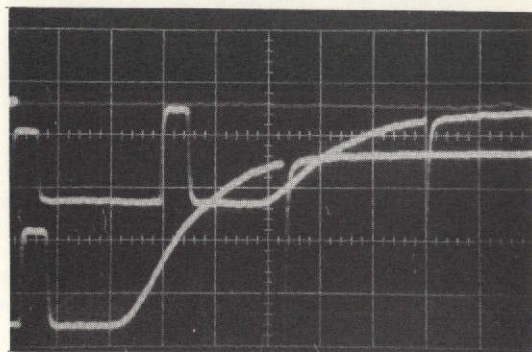
PARTICLE VELOCITY: 51.8 km/sec
MASS: 2.08 x 10^{-18} kg
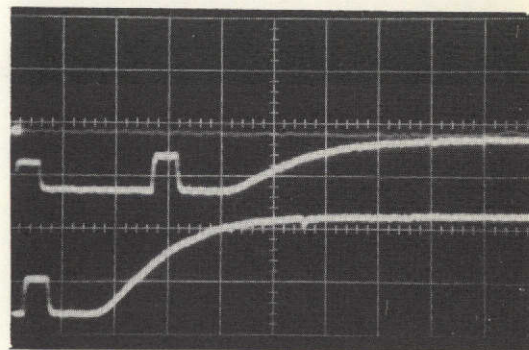TARGET PRESSURE: 1.0 x 10^{-3} Torr

(a)
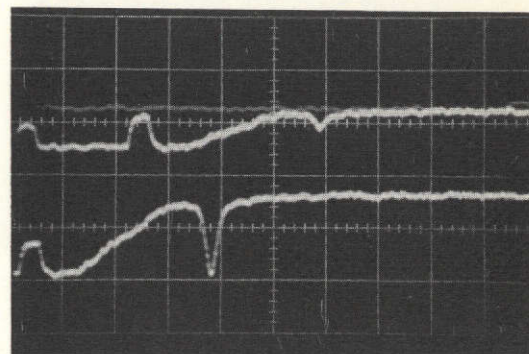
PARTICLE VELOCITY: 51.3 km/sec
MASS: 1.30 x 10^{-18} kg
TARGET PRESSURE: 1.5 x 10^{-3} Torr

(b)

PARTICLE VELOCITY: 19.4 km/sec
MASS: 7.21 x 10^{-17} kg
TARGET PRESSURE: 3.0 x 10^{-2} Torr

(c)

PARTICLE VELOCITY: 21.4 km/sec
MASS: 2.20 x 10^{-17} kg
TARGET PRESSURE: 3.0 x 10^{-2} Torr

(d)

Figure 3-3.   Oscilloscope Photographs Showing Typical Signal Response
at 20 km/sec and 50 km/sec.

ion signal indicates the spread in arrival time of the ions formed by the ablating particle.

Figure 3-3c indicates a lower velocity particle with $v = 19.4$ km/sec, $m = 7.21 \times 10^{-17}$ kg, $P_o = 3 \times 10^{-2}$ Torr. Here the mean free path in the gas is much shorter. The result is no observable ion current signal. One sees only the large amplitude negative spike caused by impact of the particle on the target.

Figure 3-3d shows a particle under almost identical conditions as those for Figure 3-3c except about 1/3 the particle mass ($v = 21.4$ km/sec, $m = 2.20 \times 10^{-17}$ kg, $P_o = 3.0 \times 10^{-2}$ Torr). This particle, for practical purposes, has evaporated within the prescribed path length. The PMT signal is present indicating ablation in the chamber and the ionization detector has produced a barely discernable step. The very small ionization detector signal shows that only a fraction of a percent of the original mass remains intact at the target plate. Figures 3-3c and 3-3d are also in an argon gas target.

Figure 3-4 represents typical data obtained at slightly higher velocity. The impact shown in Figure 3-4a was obtained with the target chamber under relatively high vacuum ($v = 91.5$ km/sec, $m = 1.99 \times 10^{-19}$ kg, $P_o < 1.0 \times 10^{-5}$ Torr). No PMT signal is observable for this event. The only signal present is the sharp negative transition of the impact ionization produced. The ionization detector for this event has a charge sensitivity of 2.85×10^{-13} coulombs per division. The output signal is differentiated with a 4.5×10^{-8} second time constant.

The photograph shown in Figure 3-4b represents an event where $v = 82.1$ km/sec, $m = 5.26 \times 10^{-19}$ kg, $P_o = 1.5 \times 10^{-3}$ Torr of argon. Here the PMT signal is observable but quite weak as is typical of the lower gas pressures. This particular particle was completely evaporated prior to reaching the impact ionization plate since no sharp transition for impact ionization is observed. The charge sensitivity in this photograph is 5.69×10^{-14} coulombs per division which is five times more sensitive than that for the impact shown in Figure 3-4a.
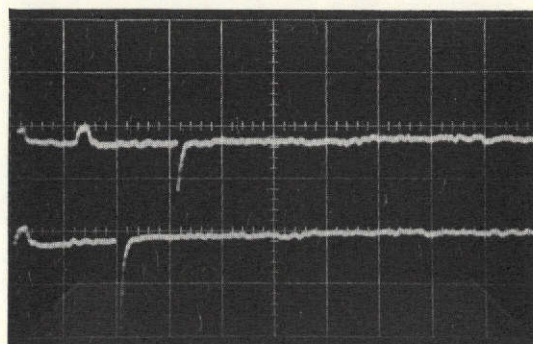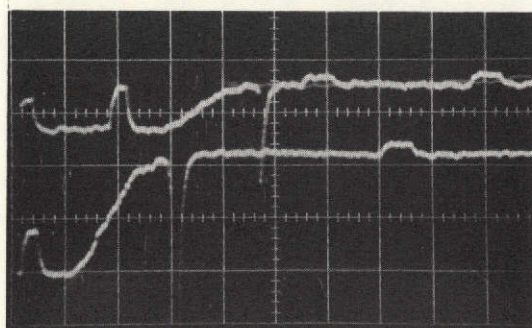
PARTICLE VELOCITY: 91.5 km/sec
MASS: 1.99×10^{-19} kg
TARGET PRESSURE: Vacuum

(a)
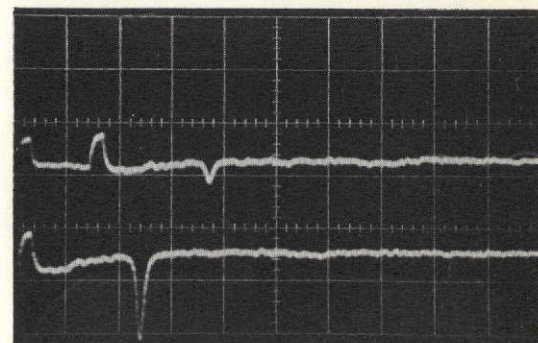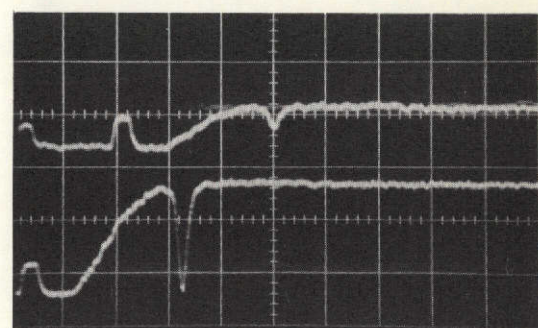

PARTICLE VELOCITY: 82.1 km/sec
MASS: 5.26×10^{-19} kg
TARGET PRESSURE: 1.5×10^{-3} Torr

(b)

PARTICLE VELOCITY: 62.6 km/sec
MASS: 1.25×10^{-18} kg
TARGET PRESSURE: 3.0×10^{-4} Torr

(c)

PARTICLE VELOCITY: 60.4 km/sec
MASS: 9.34×10^{-19} kg
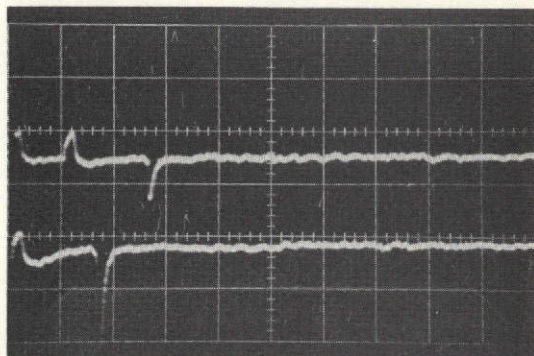TARGET PRESSURE: 1.0×10^{-3} Torr

(d)

Figure 3-4.   Oscilloscope Photographs Showing Typical Signal Response
at 60 km/sec, 82 km/sec and 91 km/sec.

Figures 3-4c and 3-4d are for comparative purposes to illustrate
a particle which failed to evaporate before reaching the target plate
(3-4c) and one which did evaporate prior to arrival at the target plate
(3-4d). Conditions are quite similar for these two cases: In (c);
$v = 62.6$ km/sec, $m = 1.25 \times 10^{-18}$ kg, $P_o = 3.0 \times 10^{-4}$ Torr of argon. In
(d); $v = 60.4$ km/sec, $m = 9.34 \times 10^{-19}$ kg, $P_o = 1.0 \times 10^{-3}$ Torr of argon.
The lower gas pressure for the case in 3-4c was clearly insufficient to
evaporate the particle as evidenced by the relatively large negative
transition for impact ionization.

The oscilloscope photographs in Figure 3-5a, b, c, and d are
for events at still higher velocity, again for comparative purposes. In
all cases, the PMT signal is weak but observable. In (a), the event is
for a particle with $v = 108$ km/sec, $m = 2.32 \times 10^{-19}$ kg and with $P_o =$
1.5×10^{-4} Torr of argon. As may be seen from the negative transition
indicating impact ionization, this particle did not completely evaporate
before hitting the target plate. The event shown in (b) illustrates
complete evaporation for $v = 116$ km/sec, $m = 1.66 \times 10^{-19}$ kg, and $P_o =$
2.5×10^{-4} Torr of argon. In (c), $v = 87.4$ km/sec, $m = 1.76 \times 10^{-19}$ kg,
$P_o = 3.0 \times 10^{-4}$ Torr of argon, incomplete evaporation is evidenced. In
(d), $v = 94.5$ km/sec, $m = 2.28 \times 10^{-19}$ kg, $P_o = 3.0 \times 10^{-4}$ Torr of argon,
complete evaporation has occurred.

As may be seen from these photographs, it becomes increasingly
more difficult to distinguish between complete and incomplete evaporation
as the velocity increases. This difficulty arises because of the reduced
time spreading of the ion group at the higher velocity. Since the chamber
pressure is reduced as the velocity increases, in order to maintain the
ablation path length (L) equal to a constant, there are fewer collisions
between evaporated particle atoms and gas molecules. This results in
less spreading in the ion group velocity and consequently a shorter rise-
time when the group impinges on the target plate. Increased bias voltage
on the impact ionization plate would eliminate this problem if it could
be made sufficiently high without initiating electrical breakdown in the
poor vacuum conditions existing in the gas target chamber. To eliminate
the ion current to the target the bias voltage would have to be capable
of stopping the highest energy ion from the particle or gas. At 100 km/sec,

PARTICLE VELOCITY: 108 km/sec
MASS: 2.32×10^{-19} kg
TARGET PRESSURE: 1.5×10^{-4} Torr
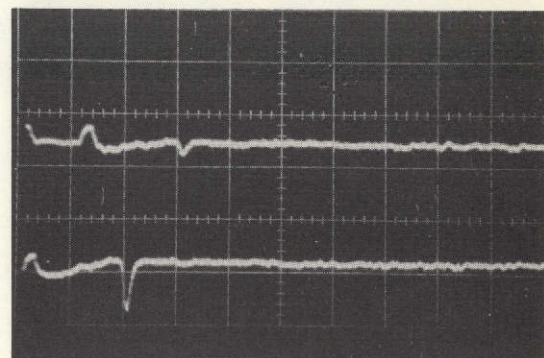
(a)
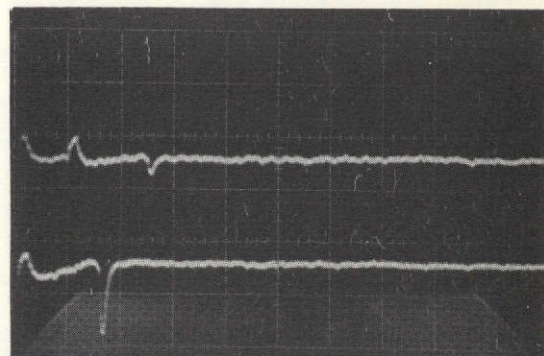
PARTICLE VELOCITY: 116 km/sec
MASS: 1.66×10^{-19} kg
TARGET PRESSURE: 2.5×10^{-4} Torr

(b)

PARTICLE VELOCITY: 87.4 km/sec
MASS: 1.76×10^{-19} kg
TARGET PRESSURE: 3.0×10^{-4} Torr

(c)

PARTICLE VELOCITY: 94.5 km/sec
MASS: 2.28×10^{-19} kg
TARGET PRESSURE: 3.0×10^{-4} Torr

(d)

Figure 3-5. Oscilloscope Photographs Showing Typical Signal Response
at 87 km/sec, 94 km/sec, 108 km/sec, and 116 km/sec.

the lanthanum atoms have approximately 7,000 electron volts of energy while the LaB_6 molecule would have about 10,000 electron volts. For the configuration used in the experiments described herein, 10 kilovolts of bias voltage was impractical.

3.3.2   Graphical Presentation of Heat Transfer Data

During the course of the program, data were obtained using LaB_6 particles in combination with target gases of air, argon and oxygen. Even though there is little to distinguish the three cases, each will be presented separately for clarity.

Due to the limitations in the technique used in obtaining the experimental data, it is not possible to make a direct calculation of the heat transfer coefficient. As will be recalled, the experiment can only tell us if the particle did or did not evaporate completely within the length of the chosen ablation path length (L). Ideally, of course, it would have been desirable to know the path length required for each individual particle. In the absence of a direct measurement of the length (L) required, Equation (8) has been utilized which is repeated here.

$$L = \frac{8\xi\rho_p r_o}{\gamma\rho_g v^2} \tag{8}$$

By rearranging the above, an expression is obtained for the initial particle radius (r_o) normalized to the gas density (ρ_g) as a function of v^2, which is

$$\frac{r_o}{\rho_g} = \frac{\gamma L}{8\xi\rho_p} v^2 . \quad \text{(variation of (8))} .$$

Since r_o/ρ_g and v^2 are measurable quantities and the path length (L), particle density (ρ_p), and total heat of ablation (ξ) are constants, then r_o/ρ_g can be plotted against v^2 with $\gamma(L/8\xi\rho_p)$ as a running parameter.

Figure 3-6 is a graph of the above with values for the heat transfer coefficient (γ) of 1.0, 0.8, 0.5 and 0.2. Superimposed on this graph is the experimental data obtained with an air target gas.
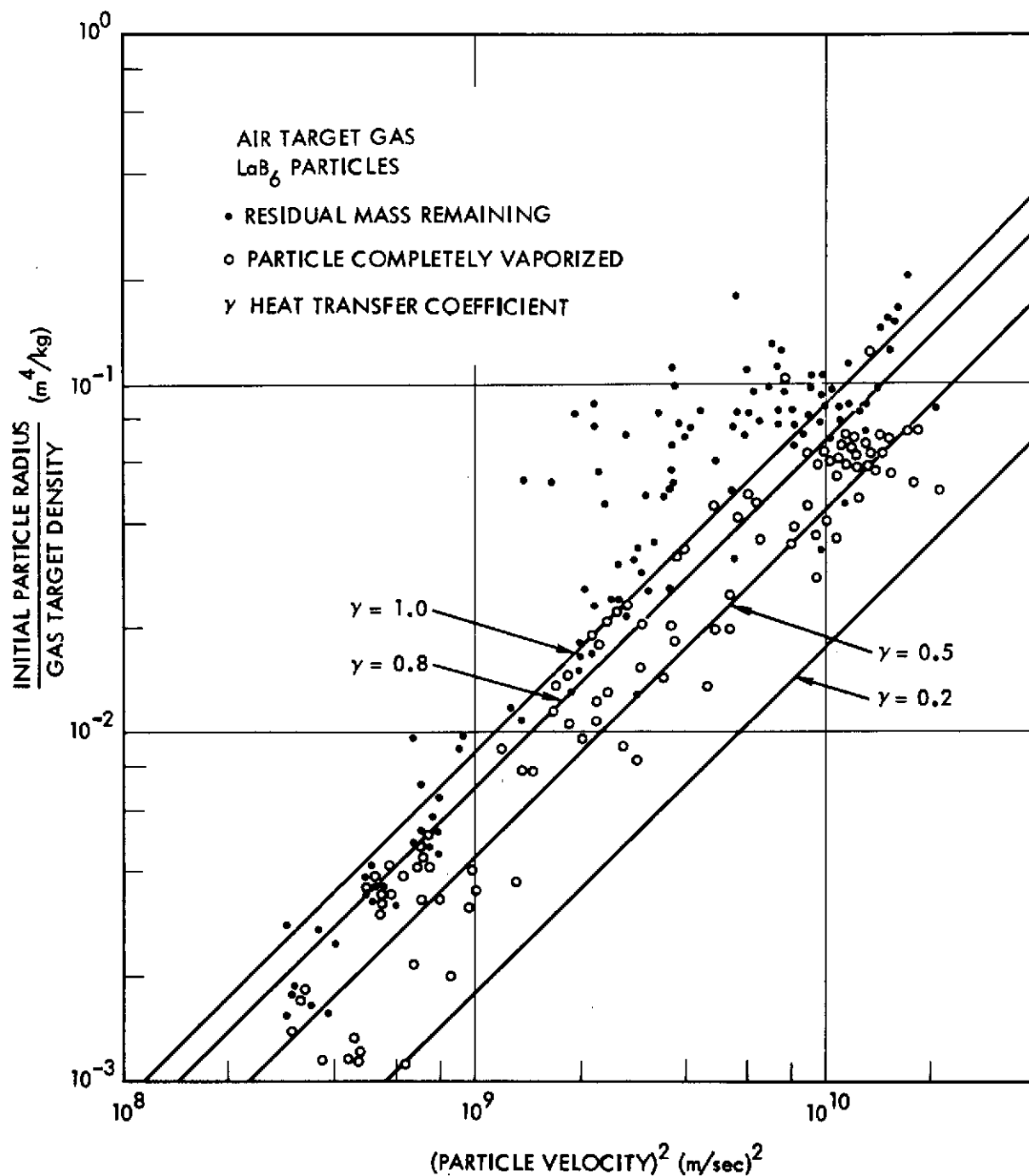
Figure 3-6. Initial Particle Radius (r_o)/Gas Target Density (ρ_g) vs Particle Velocity Squared for an Air Target Gas.

For each event recorded, the value of r_o/ρ_g and the particle velocity (v) were computed which defines a point upon the graph. The impact ionization detector then provides a flag to identify whether that particular particle was completely vaporized (an open circle on the graph) or had some residual mass remaining (a closed circle on the graph). Intuitively then, the plot should show no events where complete evaporation occurred above the line for $\gamma = 1.0$ since this would require more energy input than was available from collision with the gas. This is seen to be the case except for three points, two of which lie sufficiently close to be within reasonable experimental error. The third point is probably a result of a particle collision with the bias screens in front of the impact ionization plate since this would also result in a zero impact ionization signal.

These data in Figure 3-6 indicate that γ has a probable value of 0.9 or greater at $v^2 = 10^9$ m^2/sec^2 and approaches unity at about $v^2 = 2.5 \times 10^9$. At $v^2 = 10^{10}$ m^2/sec^2, the value of γ appears to decline toward 0.8. This is believed to be caused by a systematic experimental error; namely, a result of charge loss on the particles before they arrive at the particle charge detector. This facility has witnessed charge loss on high velocity particles on several occasions before. It is known to be more severe with increasing particle velocity and with increasing pressure in the particle accelerator tube and in the drift space where the transit time detectors are located. Every effort was made to maintain the highest possible vacuum for the experiment but the data indicate a problem still exists. The charge loss is most likely due to sputtering caused by the impacting gas molecules or by charge exchange with molecules which are adsorbed for a brief period before they are expelled from the surface. The measurement of particle charge less than that on the particle at the time acceleration took place will result in the calculation of a smaller particle radius. The effect of this is to move the position of a plotted point downward on the graph in Figure 3-6.

Figure 3-7 is a similar plot of the data acquired using argon gas in the target chamber. Here we have four data points lying well above the line $\gamma = 1.0$ which show complete evaporation. Again, these points are attributed to collision with the target bias screens and should be rejected. These data also indicate the value of γ to be 0.9 or greater
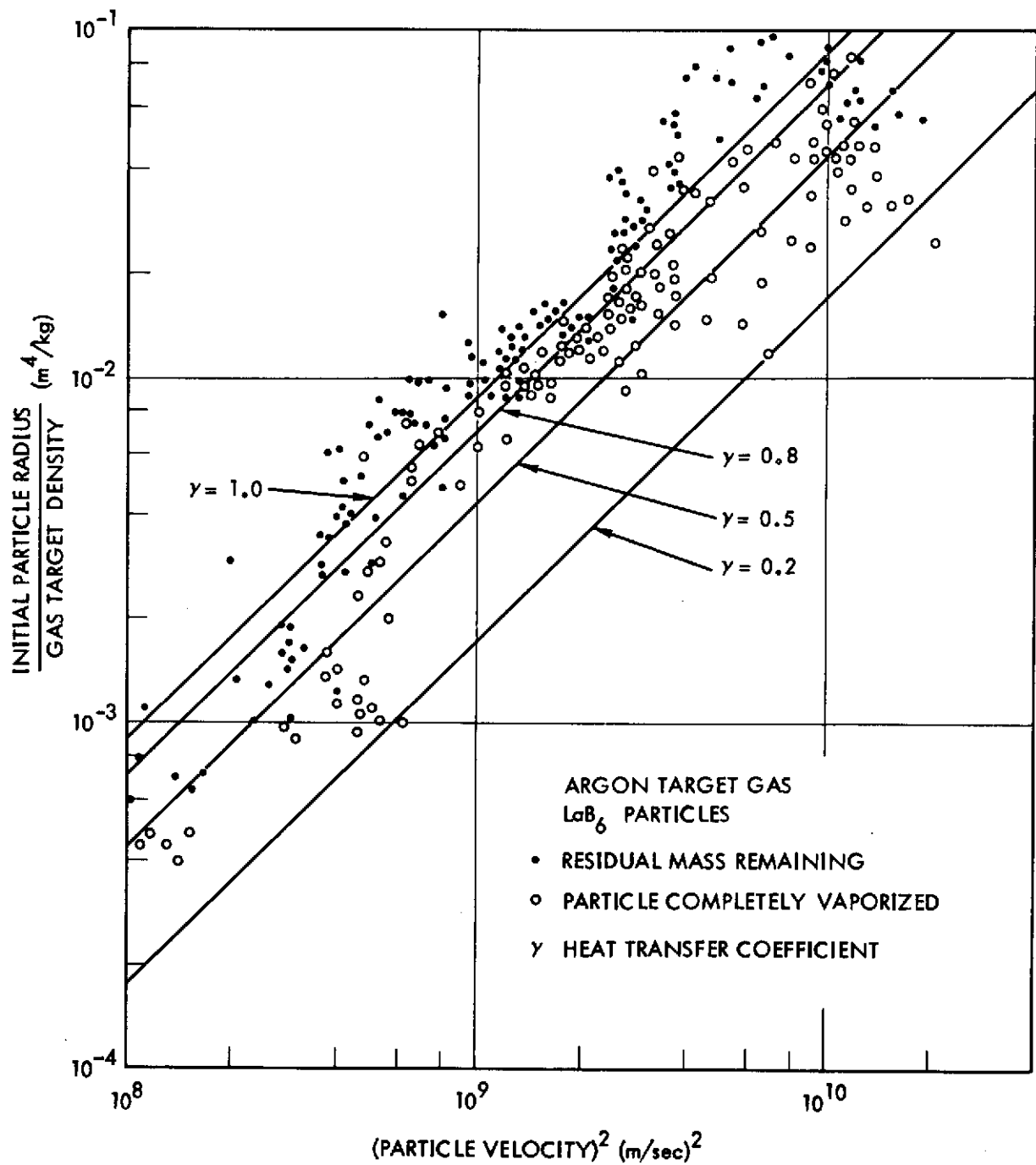
Figure 3-7. Initial Particle Radius (r_0)/Gas Target Density (ρ_g) <u>vs</u> Particle Velocity Squared for an Argon Target Gas.

at $v^2 = 10^9$ m^2/sec^2 and approaches unity at $v^2 = 2.5$ to 3×10^9 m^2/sec^2. Again the closed circles dropping to $\gamma = 0.5$ above $v^2 = 10^{10}$ m^2/sec^2 is attributed to charge loss on the particle. At the lower velocity end, $\gamma \simeq 0.8$ at $v^2 = 5 \times 10^8$ m^2/sec^2 dropping to $\gamma \simeq 0.5$ at $v^2 = 10^8$ m^2/sec^2. It should be noted that Equation (8) used to plot the running parameter (γ) was derived by assuming that the particle velocity remains essentially constant over the ablation path length. This is true to a very good approximation at the higher velocities but this assumption will begin to introduce errors as the incident particle velocity is reduced. A more rigorous derivation should be performed in which the drag equation is introduced to eliminate this source of error.

Figure 3-8 shows the data obtained using an oxygen target gas. These data are quite similar to the two cases previously described and should require no further comments.
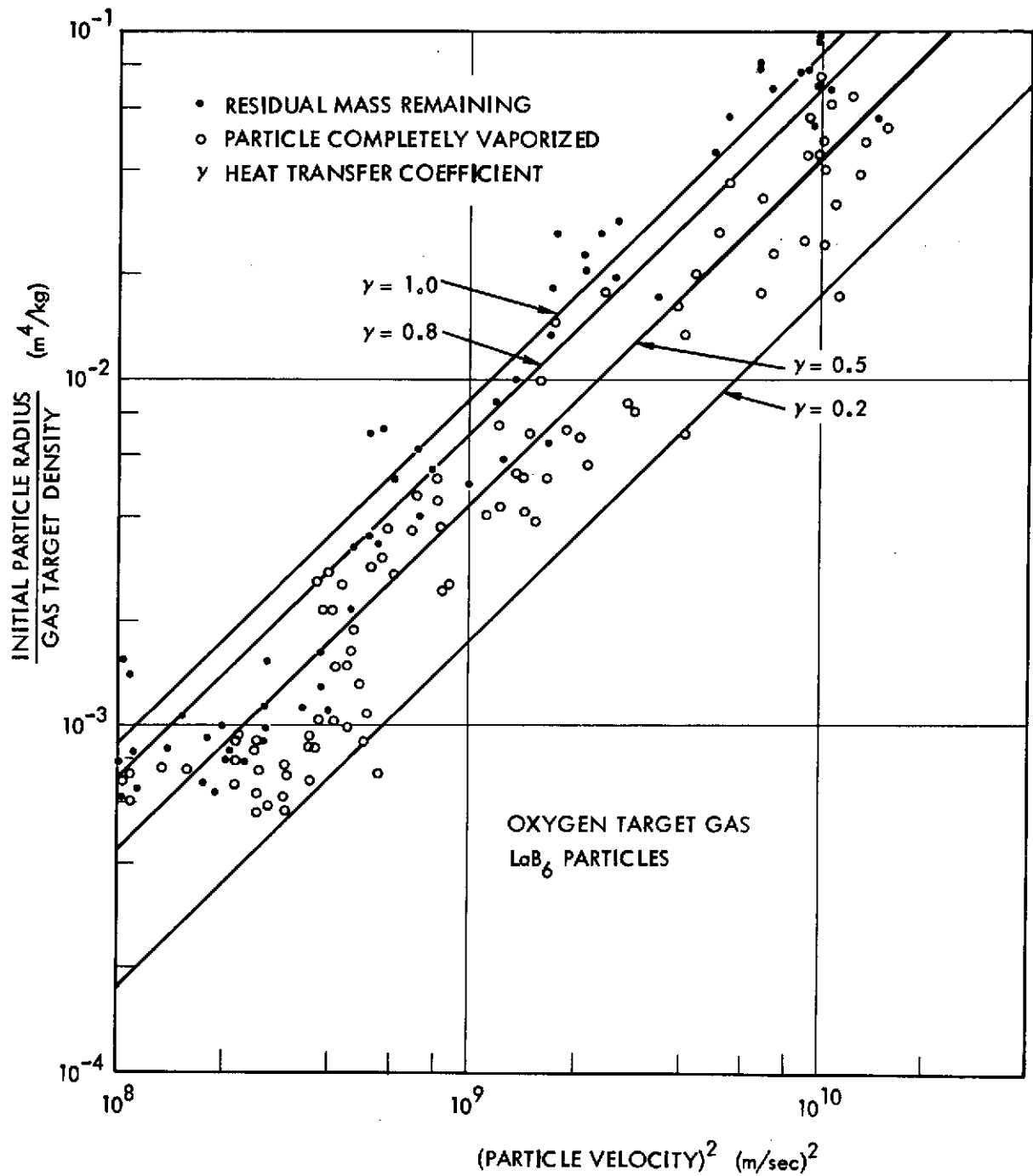
Figure 3-8. Initial Particle Radius (r_0)/Gas Target Density (ρ_g) vs Particle Velocity Squared for an Oxygen Target Gas.

4.0   SMALL PARTICLE DETECTORS

4.1   Discussion

The detection of small particles in space has been of consider-
able interest for many years. As a result of this interest a variety of
small particle detectors have been conceived and developed and have pro-
vided much desired information regarding micrometeoroid flux. Recently,
Hemenway[9] has suggested that sub-micron particles may be emitted from
the sun. This proposal comes as a result of small particle collection
experiments in the upper atmosphere where he reports finding particles
of heavy atomic weight (Hf, Ta, La, W, Tm) which are difficult to
attribute to other origins. He postulates that these heavy element, high
melting point substances could be condensed in the solar atmosphere and
then expelled presumably by radiation pressure. This hypothesis is
difficult to refute or support in a quantitative sense due to the complex-
ity of describing the formation mechanism. However, the theory could be
put to a test by flying a sunward looking small particle detector with
sufficient sensitivity to detect particles with dimensions of the order
of 0.1 micron or less.

Two such detector types appear to have favorable characteristics
for this function: The first is a solid state capacitor-type detector.
This detector is formed using semiconductor metal-oxide-silicon (MOS)
technology. Typically, a layer of silicon dioxide is grown by thermal
diffusion on a low resistivity silicon substrate to form the dielectric
of the capacitor. The silicon substrate is then one plate of the capacitor
and a thin layer of aluminum is deposited over the silicon dioxide to form
the second plate of the capacitor. When properly biased electrically, a
microparticle which penetrates the thin aluminum layer and the silicon
dioxide dielectric will initiate an electrical breakdown thereby dis-
charging the capacitor. This type of detector is considerably more rugged
than other types of thin film capacitors. The second type of detector
utilizes impact ionization to produce the detected signal. In its
simplest form it consists of a target plate, typically of high density
high melting point material, and a biasable grid over the surface which is
spaced apart some distance from it.

Both detectors mentioned above are rugged by nature and appear to offer the sensitivity which may be required. The impact ionization type detector appears to offer the greatest sensitivity and reliability.

4.2   Impact Tests With Capacitor Type Detector

The capacitor type detector discussed in Section 4.1 above has been extensively tested and the results reported.[10] However, it was felt that the tests might be extended to higher velocities than previously reported by using the TRW Micrometeoroid Accelerator. Pursuing this objective a sample of the two inch diameter detector reported in reference 10 with a 4000 $\overset{\circ}{A}$ silicon dioxide layer and with a 1500 $\overset{\circ}{A}$ aluminum film was obtained.[11] The front aluminum film was grounded and the silicon substrate was biased to -50 volts through a 1.0 megohm resistor. The signal from the capacitor active element was buffered by an amplifier before being applied to the oscilloscope input.
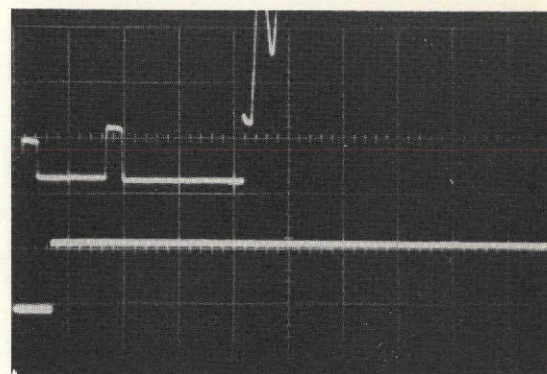
Figure 4-1 shows four oscilloscope photographs which are typical of all the breakdown signals recorded. The event shown in (a) is the lowest velocity particle impact recorded, v = 0.614 km/sec, m = 4.89 x 10^{-13} kg. The lower trace is the capacitor signal which can be seen as a positive step toward the right side of the picture. The upper trace contains the two particle detector signals from which particle charge and velocity are obtained, and also the capacitor signal. The capacitor signal appears to be noisy on the upper trace. The large signal which goes off screen and which is superimposed on the capacitor signal is actually caused by charge, liberated by the electrical break-down, traveling back upstream and collected on the last particle charge detector.

Figure 4-1b shows a particle impact with v = 6.76 km/sec, m = 6.22 x 10^{-16} kg. Figure 4-1c is for a particle with v = 17.1 km/sec, m = 5.60 x 10^{-17} kg. Figure 4-1d is the highest recorded event which produced a breakdown signal (v = 33.9 km/sec, m = 7.90 x 10^{-18} kg). In all cases, for the above photographs and for all other breakdown events, the output signal from the amplifier showed amplifier saturation which means that the input signal from the capacitor exceeded 1.0 volts.
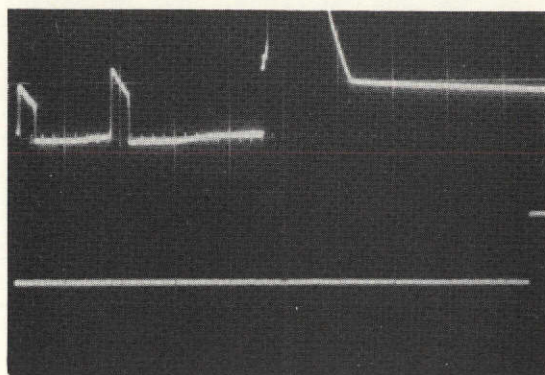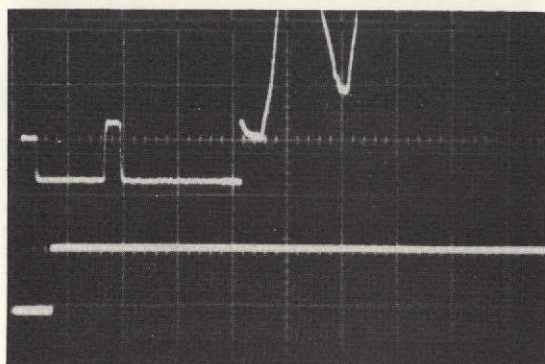
PARTICLE VELOCITY: 0.614 km/sec
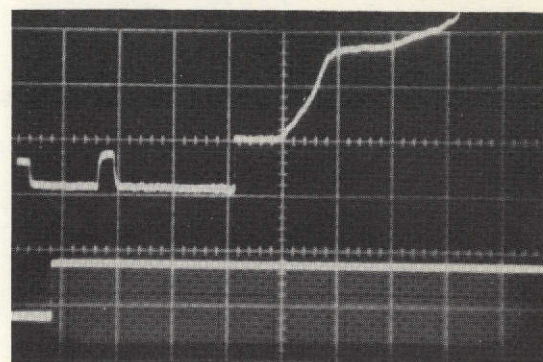MASS: 4.89 x 10^{-13} kg

(a)

PARTICLE VELOCITY: 6.76 km/sec
MASS: 6.22 x 10^{-16} kg

(b)

PARTICLE VELOCITY: 17.1 km/sec
MASS: 5.60 x 10^{-17} kg

(c)

PARTICLE VELOCITY: 33.9 km/sec
MASS: 7.90 x 10^{-18} kg

(d)

Figure 4-1. Oscilloscope Photographs Showing Signal Response From the
            Capacitor Type Detector.

Figure 4-2 is a plot of all impact events recorded with this detector. The particle radius is plotted as a function of particle impact velocity (normal incidence). A discharge signal for that event is identified by a closed circle. A no-signal event is recorded by an open circle. The slope of the curve generated by the many events recorded has no significance except to indicate the particle radius available from the accelerator as a function of velocity. The significant point is that this detector responds to the particle radius shown at velocities to almost 30 km/sec. This velocity is almost three times that previously reported in the reference cited. Note that the radius at 25 km/sec, which produced a number of breakdown signals, is 1.0×10^{-7} meters.

4.3   Impact Tests With Impact Ionization Type Detector

The impact ionization test results presented in this section were obtained using the detector described for the heat transfer measurements. As will be recalled, the target plate was tungsten. The net bias voltage for these tests was 300 volts.

Figure 4-3 shows typical ionization signals produced across the velocity range tested. Figure 4-3a shows the impact of a particle with $v = 4.26$ km/sec, $m = 2.42 \times 10^{-15}$ kg. The total collected charge was 5.35×10^{-13} coulombs. The upper trace displays the two particle detector signals and the impact ionization signal. The lower trace is at a faster sweep speed (10 microseconds/division) and shows only the impact ionization signal. Note here that the signal produced has two components in the risetime. This is typical of all events below about 5 km/sec and is attributed to the contriubtion of spray particles which go out and hit the grid thereby producing charge which is then collected on the target plate.

In (b) an event is shown for a particle with $v = 5.86$ km/sec and $m = 6.98 \times 10^{-16}$ kg. The total collected charge was 7.00×10^{-13} coulombs. Note that the two step risetime phenomena is no longer present. In (c) the impact ionization is shown for a particle impact with $v = 86.2$ km/sec, $m = 2.83 \times 10^{-19}$ kg. The total collected charge was 1.75×10^{-12} coulombs. Note that although the particle mass is almost three orders of magnitude less than in (b) the total charge is twice as large.
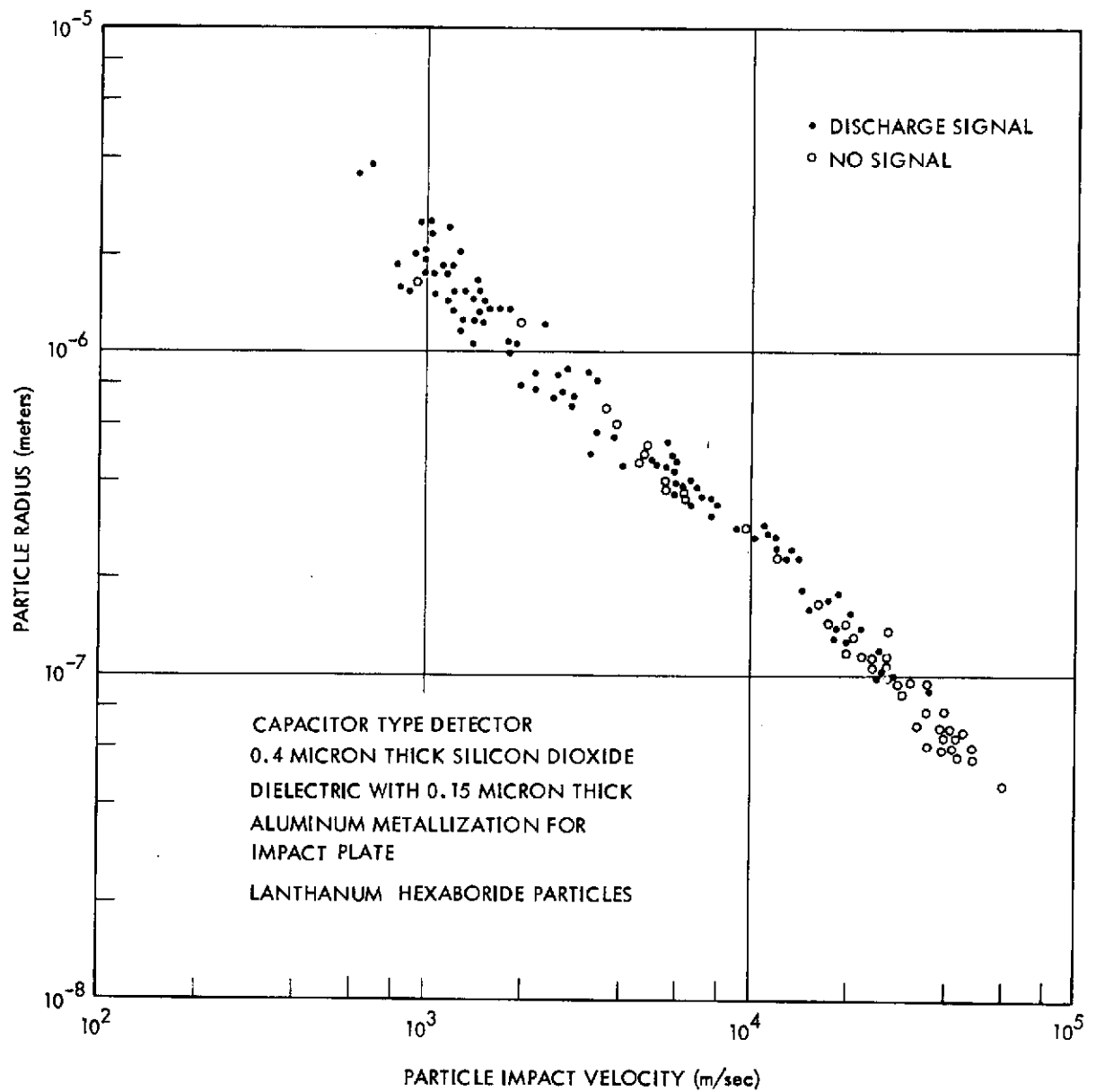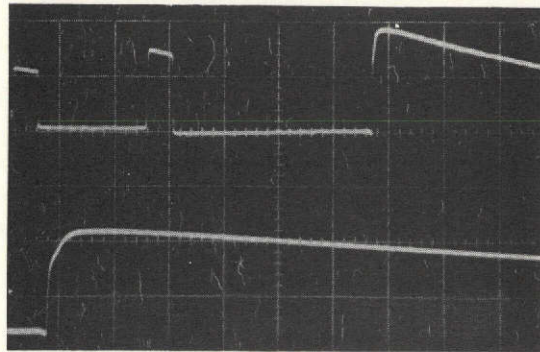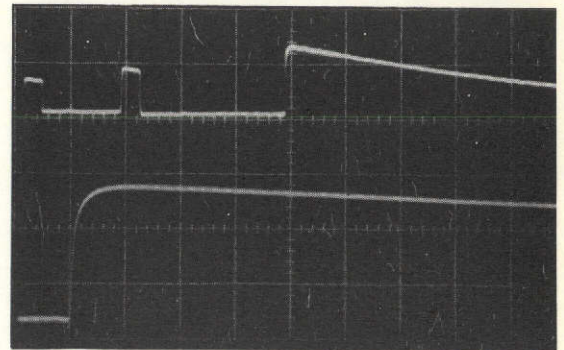
Figure 4-2. Particle Radius vs Particle Velocity Showing Response of
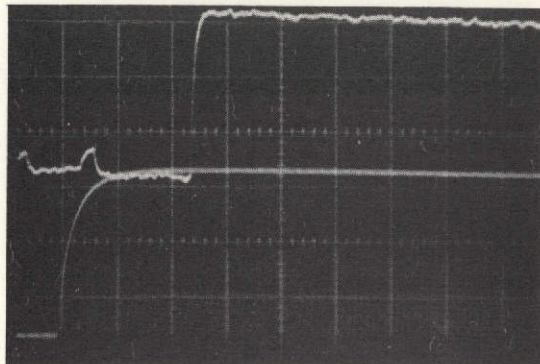Capacitor Type Detector.

PARTICLE VELOCITY: 4.26 km/sec
MASS: 2.42 x 10^{-15} kg
COLLECTED CHARGE: 5.35 x 10^{-13} Coul

(a)

PARTICLE VELOCITY: 5.86 km/sec
MASS: 6.98 x 10^{-16} kg
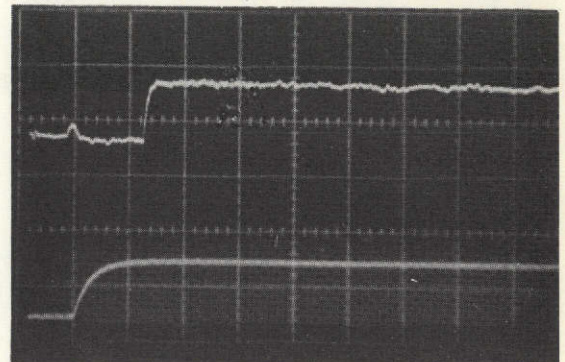COLLECTED CHARGE: 7.00 x 10^{-13} Coul

(b)

PARTICLE VELOCITY: 86.2 km/sec
MASS: 2.83 x 10^{-19} kg
COLLECTED CHARGE: 1.75 x 10^{-12} Coul

(c)

PARTICLE VELOCITY: 129 km/sec
MASS: 7.47 x 10^{-20} kg
COLLECTED CHARGE: 1.16 x 10^{-12} Coul

(d)

Figure 4-3. Oscilloscope Photographs Showing Signal Response From the
Impact Ionization Detector.

The event shown in (d) is for a particle with v = 129 km/sec, m = 7.47 x 10^{-20} kg. The total collected charged was 1.16 x 10^{-12} coulombs. The risetime of the signal is limited by the amplifier used at about 200 nanoseconds.

The data obtained from all impact ionization tests are shown in Figure 4-4. Here the total collected chrage per unit particle mass is plotted against particle impact velocity. The data obtained from this series of tests extends the velocity range by almost a factor of two above that previously tested.[4] The higher velocity tested has shown a two component curve for impact ionization not previously observed. Below 10 km/sec the normalized charge (Q_c/m_p) can be well represented by the function, $Q_c/m_p = 0.2 \ v^{4.40}$. Above 10 km/sec it may be represented by a second function, $Q_c/m_p = 1.2 \ v^{3.31}$.

The graph displayed in Figure 4-4 shows clearly the extreme sensitivity of the impact ionization type detector to high velocity microparticles. At 100 km/sec the ionization produced is 5 x 10^6 coulombs per kilogram. Assuming a reasonable detector noise level of 5 x 10^{-15} coulombs, then the detector should respond to a mass on the order of 10^{-21} kg at 100 km/sec.
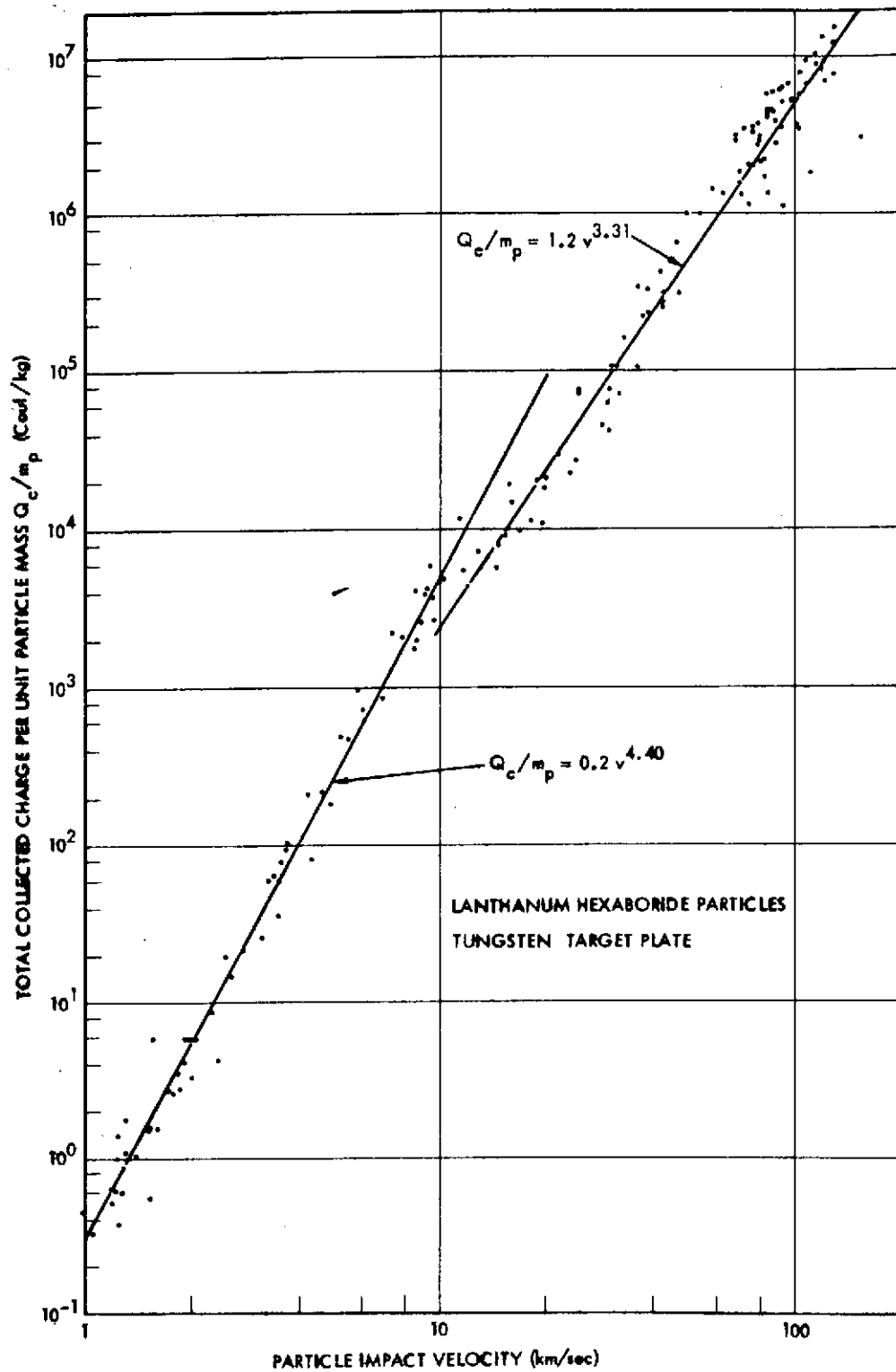
Figure 4-4. Total Collected Charge Per Unit Particle Mass (Q_c/m_p) vs
Particle Impact Velocity.

5.0   SUMMARY

The tests conducted to measure the heat transfer coefficient (γ) for particles in unshielded impact (free molecule flow) have indicated the value of γ to be approximately 0.9 or greater at 30 km/sec and approaches unity at 50 km/sec. Although the data show rolloff over 100 km/sec, this is believed to be systematic experimental error and should be disregarded. The data as plotted show γ to decrease in value to about 0.5 at v = 15 km/sec. However, the equations used for the determination of γ assume constant particle velocity over the ablation path length. This assumption introduces a source of error at lower velocities. The data should therefore be corrected by introducing the drag equation into the derivation of the equation to determine γ for values of γ below 30 km/sec.

The values of γ found above are believed to be valid ones, especially in the high velocity range of 30-70 km/sec. Although these values seem to provide the remaining essential ingredient for initial estimates for some of the micrometeoroid observables, particularly residual particulates, time did not permit these estimates to be made under the present program.

Sputtering is still an area not too well defined in relation to high velocity microparticles, although a survey of published data indicates the sputtering coefficient is sufficiently low, for the molecular energies involved, to be of little importance to those particles which undergo ablation in the upper atmosphere. On the other hand, for those micrometeoroids which are sufficiently small not to reach ablation temperatures, then sputtering can be of primary significance in determining atom and ion deposition.

The impact tests on the capacitor type detector showed the unit to have exceptionally good sensitivity for impact of sub-micron particles. The velocity tested extended to over 30 km/sec and served to show that the device should not be used to detect particles with radii below 10^{-7} meters. However, when the relatively thick dielectric (4000 Å) and aluminum layers (1500 Å) are considered it would appear that the detector can be made adequately sensitive to particles well below 10^{-7} meters radius if these two layers are made thinner.

The tests with the impact ionization type detector extended to a velocity of 150 km/sec. The slope of the normalized ionization curve was found to change slope at about 10 km/sec for the particle and target material tested. The extreme sensitivity of this type of detector would appear to make it a prime candidate for a mission to test Hemenway's hypothesis that particles are emitted from the sun. As stated previously, Hemenway's collection experiments have indicated the presence of heavy element, high melting point substances in the upper atmosphere which are suggested to have a solar origin. Although at present theory appears inadequate to quantify a formation mechanism and resulting rates of emission, a sunward-looking detector of the impact ionization type could detect such particles to extremely small dimensions should they exist. The incorporation of an ion time-of-flight spectrometer to mass analyze the charge produced would simultaneously identify the chemical composition of the impacting particle. Therefore, if the particles detected are heavy element, high melting point substances as suggested, they could be differentiated with ease from those which are of ordinary meteoric origin.

REFERENCES

1. Friichtenicht, J. F.: Evaporation of High-Velocity Particles in
    Free Molecule Flow. AIAA Journal, vol. 7, no. 4, pp 598-601, April,
    1969.

2. Samsonov, G. V.: High-Temperature Compounds of Rare Earth Metals
    with Nonmetals. Consultants Bureau, New York, 1965.

3. Friichtenicht, J. F.; and Slatter, J. C.: Ionization Associated with
    Hypervelocity Impact. NASA TN D-2091, 1963.

4. Friichtenicht, J. F.; Roy, N. L.; and Moede, L. W.: Cosmic Dust
    Analyzer. TRW Systems Group Report 10735-6002-RO-00 (Contract
    NAS9-9309, Final Report), March, 1971.

5. Friichtenicht, J. F.: Two-Million-Volt Electrostatic Accelerator
    for Hypervelocity Research. Rev. of Sci. Instr., vol. 33, no. 2,
    pp. 209-212, February, 1962.

6. Shelton, H.; Hendriks, C. D.; and Wuerker, R. F.: Electrostatic
    Acceleration of Microparticles to Hypervelocities. Journ. of
    Appl. Phys., vol. 31, no. 7, pp. 1243-1246, July, 1960.

7. Roy, N. L.; and Becker, D. G.: A Time Interval Selector and Pro-
    portional Delay Generator. Rev. of Sci. Instr., vol. 42, no. 2,
    pp. 204-209, February, 1971.

8. Hansen, D. O.; and Roy, N. L.: A Solid-State Low-Noise Preamplifier.
    Nuclear Instruments and Methods, vol. 40, pp. 209-212, North-Holland
    Publishing Co., Amsterdam, 1966.

9. Hemenway, C. L.; Erkes, J. W.; Greenberg, J. M.; Hallgren, D. S.;
    and Schmalberger, D. C.: Do Some of the Sub-Micrometer Cosmic Dust
    Particles Come From the Sun?, COSPAR Space Research XIII., Volume 2.

10. Kassel, Jr., P. C.: Characteristics of Capacitor-Type Micrometeoroid
    Flux Detectors when Impacted With Simulated Micrometeoroids. NASA
    TN D-7359, November, 1973.

11. The capacitor type detector was furnished by Jose Alvarez of NASA
    Langley Research Center, Hampton, Virginia.